学位論文

Doctor's Thesis

Usefulness of Multi-slice CT in cardiac imaging: fusion imaging, optimal contrast application and myocardial bridging

(MSCT の心臓評価における有用性: 融合画像, 至適造影プロトコール, 心筋ブリッジについて)

著者名　　中浦　猛　　Takeshi Nakaura

指導教官名　　山下　康行

審査委員名

生体情報分析医学講座教授	安東　由喜雄
心臓血管外科教授	川筋　道雄
生体機能病態学講座教授	児玉　公道
薬物治療設計学講座教授	光山　勝慶

2007 年 3 月

Contents

Multislice CT (MSCT) is gaining clinical acceptance for cardiac imaging owing to improved temporal and spatial resolution of the latest 16-slice and 64-slice technology. Although the cardiac MSCT applications are promising, there is still room for further technical improvements and optimization of techniques for cardiac evaluation.

Interestingly, the data acquired for CT angiography of the coronary arteries contain the true three-dimensional data, and we can use this data for anatomical navigation mark for perfusion imaging. Additionally, this data can also used to evaluate the surrounding myocardium such as myocardial bridging. And there is no previous report suggests that the optimal contrast injection protocols for coronary CT aingiography for 64-row MSCT.

The purpose of our study were as follows: 1) to determine the optimal view for 3-dimensional fusion image between coronary CT angiography and SPECT in the diagnosis of ischemic heart diseases; 2) to determine the optimal contrast injection protocols for coronary CT aingiography for 64-row MSCT; 3) to clarify whether myocardial bridging has some relationship for progression of atherosclerotic plaque of the proximal segment of the LAD.

Publication list

First author (corresponding author)

1. Nakaura, T, Utsunomiya D, Shiraishi, S, Tomiguchi, S, Honda, T, Ogawa, H, Awai, K, Yamashita, Y. Three-Dimensional Cardiac Image Fusion Using New CT Angiography and SPECT Methods. **Am J Roentgenol.** 185(6): 1554-1557, 2005.
2. Nakaura, T, Utsunomiya, D, Shiraishi, S, Tomiguchi, S, Kawanaka, K, Honda, T, Awai, K, Yamashita, Y. Fusion Imaging Between Myocardial Perfusion Single Photon Emission Computed Tomography and Cardiac Computed Tomography. **Circulation.** 112(3): e47-48, 2005.
3. Nakaura, T, Awai, K, Yamashita, Y. Incidence of Myocardial Bridging Observed on MDCT. **Am J Roentgenol.** 187(6): e48, 2006.

Co-author

1. Utsunomiya, D, Nakaura, T, Honda, T, Shiraishi, S, Tomiguchi, S, Kawanaka, K, Morishita, S, Awai, K, Ogawa, H, Yamashita, Y. Object-Specific Attenuation Correction at SPECT/CT in Thorax : optimization of respiratory protocol for image registration. **Radiology.** 237(2): 662-669, 2005.
2. Utsunomiya, D, Tomiguchi, S, Awai, K, Shiraishi, S, Nakaura, T, Yamashita, Y. Mutidetector-row CT and quantitative gated SPECT for the assessment of left ventricular function in small hearts: the cardiac physical phantom study using a combined SPECT/CT system. **Eur Radiol.** 16(8): 1818-1825, 2006.
3. Utsunomiya, D, Awai, K, Sakamoto, T, Nishiharu, T, Urata, J, Taniguchi, A, Nakaura, T, Yamashita, Y. Cardiac 16-MDCT for Anatomic and Functional Analysis: Assessment of a Biphasic Contrast Injection Protocol. **Am J Roentgenol.** 187(3): 638-44, 2006.

Acknowledgements

These academic investigations were done during my postgraduate period from 2002 to 2006 at department of Diagnostic Radiology.

I wish to extend my sincere thanks to Professor Yasuyuki Yamashita, Chairman of the Department of Diagnostic Radiology Graduate School of Medical Sciences, Kumamoto University for general guidance and constructive instructions.

I am deeply grateful to Professor Kazuo Awai, chairman of Department of Diagnostic Radiology Graduate School of Medical Sciences and to Professor Seiji Tomiguchi, chairman of Department of Health Sciences Graduate School of Medical Sciences, who has instructed me during the process of my study.

Of course, I owe a great deal to the colleagues of radiology, Dr. Nakayama, Dr. Yanaga, Dr. Ikeda and Dr. Shiraishi.

Finally special thanks are due to Professor Hisao Ogawa, chairman of Department of Cardiovascular Medicine, Kumamoto University School of Medicine for full support.

Chapter I Optimal view for cardiac fusion imaging

Preliminary study

Before this clinical study, we performed a preliminary study with one patient who had the history of an acute myocardial infarction with left anterior descending artery stenosis and had undergone percutaneous transluminal coronary angioplasty and coronary stenting (Figure 1). ECG-gated cardiac 8-slice CT angiography and thallium stress test were performed in a combined single photon emission computed tomography (SPECT) - CT system (Figure 2), and we evaluated the various 3-dimensional reconstructed SPECT images.

Because workstation for SPECT data have only maximum intensity projection (MIP) function, all of the CT and SPECT images were sent to a PC for registration and conversion by using original programs written in the Borland Delphi computer language.

First, we evaluated the colored Ray-Sum and MPR (Figure 3), but the relationship between the myocardial perfusion defect and coronary artery was equivocal. And this method requires manual interpretation and mental integration of many images by the reviewer.

Second, we evaluated the 3D volume rendering view. We reconstructed all images of SPECT to CT format as other series of CT angiography using a original program, and transferred all data to CT workstation. The perfusion defect is clearly depicted as compared with MIP image (Figure 4), and the fused images (Figure 5) showed a perfect match between the left anterior descending artery territory and the defect of tracer uptake.

Then, we determined the 3D-volume rendering view is optimal for fused image between coronary CT angiography and myocardial SPECT.

Abstract

OBJECTIVE: The purpose of this study was to develop a method of fused images of coronary CT angiography and myocardial perfusion SPECT.

CONCLUSION: Four patients with ischemic heart disease underwent 3D volume-rendering fused images using a conversion program and volume-rendering fusion function of a computer workstation. The fusion images clearly showed the relationship of relevant coronary arteries and the abnormal perfusion territory in all patients and were useful for the evaluation of coronary artery disease.

Introduction

The integration of anatomic and physiologic information from coronary angiograms and myocardial SPECT images may be useful for the clinical assessment and effective treatment of coronary artery disease (CAD). Recent advances in computer technology allow the 3-dimensional (3D) demonstration of the coronary artery tree from computed tomograms (CT). We have developed a method to integrate the information from 2 non-invasive cardiac imaging studies, myocardial perfusion SPECT and coronary CT angiography. This technique obviates the need for knowledge of the relationship between the anatomical lesion in the coronary artery tree and the corresponding myocardial segment with perfusion abnormality.

Materials and Methods

Four consecutive patients with CAD were enrolled in this study approved by the institutional review board. They were 3 men and a woman; their ages ranged from 65 to 81 years (mean 73.5). All underwent thallium-201 myocardial SPECT imaging and coronary CT angiography with a combined SPECT/MDCT system that consisted of a 2-head gamma camera (Skylight, ADAC, Milpitas, CA) and an 8 detector-row MDCT (Lightspeed Ultra, GE, Milwaukee, WI). They were juxtaposed so that the CT table bearing the patient could be moved directly into the gamma camera. Three of them also underwent coronary angiography.

Stress SPECT images were acquired 5 min after the injection of thallium-201 (111 MBq). Coronary CT angiograms were obtained immediately after the stress SPECT study without changing the patient's position on the table. Delayed SPECT images were acquired 3-4 hr later. SPECT images were obtained using low-energy general-purpose parallel-hole collimators with an electrocardiography (ECG) gating at 8 frames per R-R interval. A 35% energy window was used to acquire the 74- and 169-keV peaks of thallium-201 and 32 step-and-shoot images (64 x 64 matrix) were acquired over 180°from a 45°right anterior oblique to a 45° left posterior oblique angle with 1 min per projection. Transaxial images of summed raw data were then reconstructed with an ML-EM algorithm using a Butterworth filter (critical frequency 0.6 cycle/cm, order 5). The slice thickness of each transaxial image was about 6 mm. Neither attenuation nor scatter correction was performed.

The CT scans were obtained using a standard ECG-gated coronary CT angiography protocol, 0.5-sec rotation time, 1.25 mm detector row width, 1.25 mm image thickness, 1.5-2.0 pitch, 120 kV, and 350 mA. A test bolus (20 ml of contrast material) (Omnipaque 300) and a chaser bolus (20 ml of saline) were used. The circulation time was determined by measuring CT attenuation values in the ascending aorta. A 100-ml bolus of contrast material was injected at 4 ml/sec; this was followed by a 30-ml chaser bolus of saline. A conventional single-sector algorithm was used when the heart rate was slower than 70 beats/min, a segmented reconstruction algorithm when it was faster than 71 beats/min. For image reconstruction we used the raw data file at 75% of

the cardiac cycle. The reconstructed slice thickness was 1.25 mm, the image increment 1.25 mm.

After image reconstruction, all CT and stress SPECT images were transferred to a personal computer for registration and conversion with computer-software developed by one of the authors (T.N.). Image registration of SPECT and CT was performed by pixel-shift manual registration using the left ventricular myocardium as an internal marker. The image corresponding to each CT slice was reconstructed from the SPECT image by linear interpolation, the output by the DICOM format as another series of CT studies. Original CT- and reconstructed SPECT images were transferred to the workstation (ZIO M900, Zio Software Inc., Tokyo, Japan) that features a volume rendering fusion function for post-processing. For shrinking by several pixels, the dispersion lines on registered SPECT images were trimmed.

Perfusion SPECT volume-rendering images were presented with a linear rainbow color scale with seven colors ranging from purple to red. This is a commonly used technique for visualization of myocardial perfusion SPECT images. The opacity curve of the color scale in relation to voxel count was set to linear upward slope.

Segmentation of the heart was performed manually from the MDCT slices. The color scale of CT angiography was that recommended for this workstation. Volume-rendering fused images were obtained from original CT- and registered SPECT images using a volume-rendering fusion function. Volume-rendering fused images were compared with CT angiograms, SPECT images alone, and coronary angiograms.

Four consecutive patients with CAD were enrolled in this study approved by the institutional review board. They were 3 men and a woman; their ages ranged from 65 to 81 years (mean 73.5). All underwent thallium-201 myocardial SPECT imaging and coronary CT angiography with a combined SPECT/MDCT system that consisted of a 2-head gamma camera (Skylight, ADAC, Milpitas, CA) and an 8 detector-row MDCT (Lightspeed Ultra, GE, Milwaukee, WI). They were juxtaposed so that the CT table bearing the patient could be moved directly into the gamma camera. Three of them also underwent coronary angiography.

Stress SPECT images were acquired 5 min after the injection of thallium-201 (111 MBq).

Coronary CT angiograms were obtained immediately after the stress SPECT study without changing the patient's position on the table. Delayed SPECT images were acquired 3-4 hr later. SPECT images were obtained using low-energy general-purpose parallel-hole collimators with an electrocardiography (ECG) gating at 8 frames per R-R interval. A 35% energy window was used to acquire the 74- and 169-keV peaks of thallium-201 and 32 step-and-shoot images (64 x 64 matrix) were acquired over 180°from a 45°right anterior oblique to a 45° left posterior oblique angle with 1 min per projection. Transaxial images of summed raw data were then reconstructed with an ML-EM algorithm using a Butterworth filter (critical frequency 0.6 cycle/cm, order 5). The slice thickness of each transaxial image was about 6 mm. Neither attenuation nor scatter correction was performed.

The CT scans were obtained using a standard ECG-gated coronary CT angiography protocol, 0.5-sec rotation time, 1.25 mm detector row width, 1.25 mm image thickness, 1.5-2.0 pitch, 120 kV, and 350 mA. A test bolus (20 ml of contrast material) (Omnipaque 300) and a chaser bolus (20 ml of saline) were used. The circulation time was determined by measuring CT attenuation values in the ascending aorta. A 100-ml bolus of contrast material was injected at 4 ml/sec; this was followed by a 30-ml chaser bolus of saline. A conventional single-sector algorithm was used when the heart rate was slower than 70 beats/min, a segmented reconstruction algorithm when it was faster than 71 beats/min. For image reconstruction we used the raw data file at 75% of the cardiac cycle. The reconstructed slice thickness was 1.25 mm, the image increment 1.25 mm.

After image reconstruction, all CT and stress SPECT images were transferred to a personal computer for registration and conversion with computer-software developed by one of the authors (T.N.). Image registration of SPECT and CT was performed by pixel-shift manual registration using the left ventricular myocardium as an internal marker. The image corresponding to each CT slice was reconstructed from the SPECT image by linear interpolation, the output by the DICOM format as another series of CT studies. Original CT- and reconstructed SPECT images were transferred to the workstation (ZIO M900, Zio Software Inc., Tokyo, Japan) that features a volume rendering fusion function for post-processing. For shrinking by several pixels, the dispersion lines on

registered SPECT images were trimmed.

Perfusion SPECT volume-rendering images were presented with a linear rainbow color scale with seven colors ranging from purple to red. This is a commonly used technique for visualization of myocardial perfusion SPECT images. The opacity curve of the color scale in relation to voxel count was set to linear upward slope.

Segmentation of the heart was performed manually from the MDCT slices. The color scale of CT angiography was that recommended for this workstation. Volume-rendering fused images were obtained from original CT- and registered SPECT images using a volume-rendering fusion function. Volume-rendering fused images were compared with CT angiograms, SPECT images alone, and coronary angiograms.

Results

3D volume-rendering fused images clearly demonstrated the relationship of a relevant coronary artery and the abnormal perfusion territory in all patients. There was no clinically problematic misregistration between CT and SPECT images on the 3D volume-rendering fused images.

As an illustrative case, we present imaging findings on a 62-year-old man with three-vessel coronary disease. He had undergone coronary artery bypass grafting; left internal thoracic artery (LITA) to left anterior descending coronary artery (LAD), LITA to left circumflex coronary artery (LCX), and right internal thoracic artery (RITA) to right coronary artery (RCA). Three weeks later he underwent postoperative examination consisting of CT angiography and myocardial SPECT. The patency of the bypass grafts was well defined on the coronary CT angiograms. Myocardial infarction in the LAD territory was defined as a defect in tracer uptake with reverse redistribution on SPECT images (Figure 1A). The 3D fused image showed a perfect match between the LAD territory and the tracer uptake defect
(Figure 1B).

Another patient with a clinical history of old myocardial infarction was suspected of ischemia. CT angiography and myocardial SPECT were performed as preoperative examinations. Myocardial SPECT showed a defect in tracer uptake in the LAD territory with partial redistribution (Figure 2A). CT angiography disclosed occlusion of segment 7 and stenosis of segment 9. The 3D fused image showed good agreement between the territory of the diseased coronary artery and the myocardial perfusion defect (Figure 2B, C). Conventional coronary angiography was performed for percutaneous transluminal coronary angioplasty (Figure 2D).

Discussion

In our pilot study, the relationship between the diseased coronary artery and the myocardial perfusion defect was clearly depicted on fused images. There was good agreement between the myocardial perfusion defect and the territory of the diseased coronary artery. There was no clinically problematic misregistration between CT and SPECT images and we were able to obtain functional and anatomical information simultaneously on one view. There was good agreement with the diseased area responsible for the blood vessel abnormalities seen on x-ray coronary angiograms.

Previous studies (1-3) showed that fusion images of coronary arteries and myocardial perfusion facilitate assessment of the hemodynamic significance of coronary stenosis. Schindler et al. (1,2), who presented a method for fusing the 3D reconstructed coronary tree and 3D myocardial perfusion distribution, subjectively determined that 74% of 162 coronary lesions from 78 patients coincided with areas of regional hypo-perfusion. Faber et al. (3), who developed a unification algorithm by nonlinear warping for automatically registering 3D models of the epicardial surface from perfusion SPECT and 3D coronary artery trees from coronary angiographs, evaluated performance in a unique patient population in which anatomic and physiologic at-risk areas could be expected to overlap. They found an 80% and 84% overlap in at-risk- and normal areas, respectively.

We propose that coronary CT angiography is more suitable than coronary angiography for image fusion. The great advantage of CT angiography is its low invasiveness; since all data are represented in true 3D formats, and because the cardiac muscle is also visualized, this can be used as an internal landmark for the image. Although the resolution of coronary arteries on CT images is much lower than on standard coronary angiograms, multi-slice CT provides clear visualization of the coronary artery.

Although in some of our cases heart beat and respiration led to misregistration between CT and SPECT images, this did not negatively affect the clinical evaluation. To eliminate misregistration attributable to the heart beat, we extracted SPECT data from a cardiac phase similar to that of the CT image (diastolic phase) from the ECG-gated SPECT data and used this as myocardial perfusion

data. However, the number of pixels corresponding to the thickness of the left ventricular myocardium on the extracted SPECT images was lower than that of summed raw SPECT images. For the display of 3D volume-rendering fused images, some pixels must be eliminated from the outer side of the left ventricular myocardium. In our study it was difficult to fuse volume-rendering CT images with diastolic SPECT images because the count density in the left ventricular myocardium was seriously distorted by the elimination of the outer pixels from the left ventricular myocardium.

Although we used the same table for both coronary CT angiographic and SPECT imaging, misregistration due to respiration was observed. To resolve this problem, rotation of CT and SPECT images in any direction and registration along the cardiac axis may be necessary. This is also important in cases where registration of CT and SPECT images occurs in different rooms.

In conclusion, fused images of coronary CT angiography and myocardial SPECT are useful for the evaluation of CAD. As they present a panoramic view of the coronary vessels and myocardial perfusion, the relationship between the diseased artery and the myocardium can be determined without requiring difficult mental integration by the evaluator.

Chapter II Optimal Contrast Media Injection Protocols for Cardiac Fusion Imaging in 64-row MSCT

Preliminary study

Before this clinical study, a preliminary study with test injection was performed to establish the time–density curve profiles with various contrast injection protocols. We retrospectively reviewed the records and images of 18 patients (average: 69.7 ± 11.8 years old, 59.9 ± 10.9 kg) who underwent CT angiography on a 40-MDCT scanner with test injection technique at ascending aorta with different injection rates.

We calculated the expected time–density curve based on the mathematical analysis of a patient's time-attenuation response to a small test-bolus injection using the simple 'additive model' reported by Fleischmann (1). The average time–density curves with various contrast injection protocols (volume of CM: 36ml, 48ml, 60ml; injection duration: 10sec, 15sec, 20sec, 25sec and 30sec) were calculated to expect the optimal injection volume and duration (Figure 1).

In this study, we hypnotize the 60ml (1.0ml/BW) / 15sec injection protocol is optimal for coronary CTA. Because it satisfied these requirement: (a) adequate enhancement of ascending aorta (about 300 HU) and (b) plateau phase of contrast enhancement.

1. Fleischmann D. High-concentration contrast media in MDCT angiography: principles and rationale. Eur Radiol 2003; 13 Suppl 3:N39-43.

ABSTRACT

Purpose: To compare patient-weight-adjusted- and fixed-contrast-dose injection protocols and fixed-dose- and fixed injection-rate protocols at coronary computed tomography angiography (CTA) using a 64-detector scanner.

Materials and Methods: Approval from our institutional review board and patient prior informed consent were obtained before entering 60 patients with suspected coronary disease in this study. The patients were randomly assigned to one of two protocols. In protocol 1 (P1) they received a fixed contrast-dose of 80 ml Iohexol-370 at an injection rate of 4.0 ml/sec. In protocol 2 (P2) the dose was tailored to the patient body weight (BW); this group received 1.0 ml/kg BW at an injection duration of 15 sec. Imaging was on a 64-detector CT scanner. Computer-assisted bolus tracking was used to synchronize the contrast injection with the start of CT scanning. Attenuation values were measured in the superior vena cava, ascending aorta, pulmonary artery, right and left ventricular cavity, left main coronary artery, and the proximal-, middle-, and distal segment of the right coronary artery. For each protocol, aortic enhancement was compared in patients with a BW<58 kg (group 1) and □58 kg (group 2). The standard deviation (SD) of CT attenuation in the aortic root and the myocardium was measured to evaluate image noise. The protocols were compared using the two-tailed Student t-test.

Results: The attenuation values for the superior vena cava and the right and left ventricular cavity were significantly higher in P1 than P2, however, there was no significant difference in the attenuation values of the ascending aorta, left main coronary artery, and the proximal-, middle-, and distal segment of the right coronary artery. The SD of the ascending aorta and myocardium was significantly higher in P1 than P2.

Conclusion: At 64-detector CTA of the heart, the patient BW-tailored dose protocol with shorter injection duration yielded significantly better image quality than the fixed-dose, 20-sec injection duration protocol.

Key Words: MDCT, contrast media, vessel enhancement, injection protocol

INTRODUCTION

Because their speed is faster, 64-detector scanners yield coronary CT angiograms (CTA) that are almost motion-free and of isotropic spatial resolution (1-5). Therefore, for the detection of coronary artery stenosis, coronary CTA obtained with 64-detector scanners may represent a reliable alternative to conventional coronary angiography. To exploit fully the diagnostic capabilities of coronary CTA, optimal enhancement of the coronary arteries is essential (6). Although several contrast enhancement protocols for coronary CTA have been reported (7-13), most were developed for 4- or 16-detector CT scanners. The 64-detector CT scanners can scan the whole heart in less than 10 sec at less than 1.0 mm sections. While shorter scan times may allow a decrease in the volume of contrast material (CM) necessary for CTA, low-dose CM protocols are sensitive to the patient body weight (BW)(14-17) and the optimal temporal scan window may be narrower, making it difficult to adjust scan timing and the optimal temporal window.

We found that at CTA of the abdominal aorta and dynamic CT of the liver, protocols that delivered contrast doses tailored to the patient BW at a fixed injection duration achieved stable aortic contrast peak time and peak enhancement (15). However, at coronary CTA, protocols using a fixed contrast dose and injection rate continue to prevail. We hypothesized that, irrespective of the patient BW, protocols with BW-adjusted contrast doses and fixed injection durations would yield adequate enhancement and scan timing at coronary CTA with a 64-detector CT scanner. The purpose of our current study was to compare BW-adjusted- and fixed contrast-dose injection protocols and fixed-dose and fixed injection-rate protocols at coronary CTA with a 64-detector CT scanner.

MATERIALS AND METHODS

This study was approved by our institutional review board. Prior informed consent was obtained from all patients after we explained the purpose of the study and that their participation would not interfere with their clinical examinations.

Patient Population

Between March and October 2006, 66 patients were considered for this prospective study. The inclusion criteria were *(a)* suspicion of coronary artery disease based on electrocardiograms or clinical symptoms, *(b)* absence of renal failure (serum creatinine > 1.5 mg/dl [114 mol/l]) or contraindication for iodinated contrast material, and *(c)* absence of severe cardiac failure (i.e. ejection fraction of the left ventricle 50% or less at echocardiography). The enrolled patients satisfied all criteria; 6 patients were excluded because they did not take nitroglycerin just before cardiac CT examination (n=3), manifested arrhythmia (n=2), or because the scan timing deviated from the scanning protocol (n=1). Consequently, 60 patients were available for assessment; they were 29 men and 31 women ranging in age from 39 to 93 years (mean 65.0 years). The men ranged in age from 39 to 90 years (mean 65.2 years), the women from 39 to 93 years (mean 64.7 years). According to the Student *t*-test there was no significant age difference between the males and females ($p = 0.90$).

Contrast Injection Protocols

In all patients, iopamidol with an iodine concentration of 370 mg/ml (Iopamiron-370; Nihon Schering, Osaka, Japan) was delivered via a 20-gauge catheter inserted into an antecubital vein and a power injector (Autoenhance A-250; Nemoto Kyorindo, Tokyo, Japan). Of the 60 enrolled patients, 30 each were randomly assigned to one of two contrast injection protocols using a random table. In protocol 1 (P1), a fixed contrast-dose protocol, they received 80 ml of CM at an injection rate of 4.0 ml/sec. Protocol 2 (P2) was a patient BW-tailored dose protocol; the patients received 1.0 ml/kg BW of CM at a fixed injection duration of 15 sec. In both protocols, contrast

administration was followed by the administration of 40 ml of saline solution delivered at the same injection rate as CM.

P1 patients ranged from 39 to 83 years (mean 62.4 years), P2 patients from 39 to 93 years (mean 67.5 years). By the Student *t*-test there was no significant difference in the age of P1 and P2 patients ($p = 0.12$). The mean BW of P1 patients was 60.1 ± 14.2 kg (range 39.5 - 100 kg), that of P2 patients was 59.5 ± 12.8 kg (range 36 - 100 kg); according to Student's *t*-test, the difference was not significant ($p = 0.86$). P1 patients were 13 men and 17 women, P2 patients were 16 men and 14 women; by the χ^2 test, the gender distribution was not significantly different ($p = 0.44$). The mean heart rate of P1 and P2 patients was 66.5 ± 12.5 (range 50 - 96) and 65.8 ± 12.9 (range 49 - 115) beats/min, respectively and by Student's *t*-test, the difference was not significant ($p = 0.82$).

Scanning and Image Reconstruction Protocol

At 5 min prior to scanning, each patient received 0.3 mg of nitroglycerin (Nitropen; Nippon Kayaku, Tokyo, Japan) sublingually to dilate the coronary arteries. All patients were scanned in the supine position during a single breath-hold with tidal inspiration during scanning on a 64–detector CT scanner (Brilliance-64; Philips Medical Systems, Cleveland, OH, USA). The parameters were: detector collimation 64 x 0.625 mm, 11.9 mm/sec table feed increments, 0.20 helical pitch (beam pitch), 420 msec tube rotation time, 120 kV tube voltage, 900 mAs tube current time-product. Depending on the cardiac dimensions, the scanning time varied from 6 to 8 sec. Image reconstruction was in a 16.5 - 20.0-cm display field of view depending on the patient's physique. These scanning parameters were the same as routinely used at our hospitals for cardiac CT. All scans were started at the upper end of the coronary sinus in a cephalocaudal direction.

A computer-assisted bolus tracking program (Bolus Pro Ultra, Philips Medical Systems) was used to synchronize CM arrival in the coronary arteries with the start of scanning (9, 18). The CT number was monitored at the level of the ascending aorta by a radiological technologist with 8 years of experience in cardiac CT; the region of interest (ROI) cursor was placed in the aorta. The

size of the ROI cursor in the abdominal aorta was 0.8 - 2.0 cm^2. Real-time low-dose (120 kVp, 60mA) serial monitoring scans were initiated 8 sec after the start of CM injection. The trigger threshold level was set at 200 Hounsfield units (HU). Scanning started automatically 6 sec after the CT number in the ascending aorta reached 200 HU. During monitor- scanning, the patients were instructed to practice shallow and regular breathing.

We reconstructed axial images with a section thickness of 0.67 mm and a section interval of 0.33 mm using a medium cardiac kernel (CB) with ECG gating. Initially, a single data set was reconstructed during the mid-diastolic phase (75% of the R-R interval). In cases with unsatisfactory image quality, image reconstruction of the raw data was performed at 0-, 10-, 20-, 30-, 40-, 50-, 60-, 70-, 80-, and 90% of the R-wave to R-wave interval to improve the image quality of all available coronary segments. We used a conventional single-sector algorithm when the heart rate was slower than 65- and a segmented cardiac reconstruction algorithm when it was faster than 66 beats per min.

Data Analysis

Attenuation in the great vessels, ventricular cavities, and coronary arteries

A board-certificated radiologist (T. N.) with 4 years of experience in cardiac CT imaging measured the attenuation values of portions described below by placing a manually defined ROI. We select 4 representative slice levels in each patient, where level 1 is the origin of the left main trunk, level 2 the origin of the right coronal artery, level 3 the center of the left ventricle, and level 4 the bifurcation of the atrioventricular node branch. The ROIs for vessels were as large as possible and papillary muscles, calcifications, plaques, and stenoses were carefully avoided. The ROIs for muscle were also as large as possible and ventricular cavities, vessels, and fat were carefully avoided. Examples of selected slices and ROIs are shown in Figs. 1a-d.

We measured attenuation of the superior vena cava, ascending aorta, pulmonary artery- and left main trunk at level 1 (Fig. 1a), of the proximal right coronary artery at level 2 (Fig. 1b), of the right- and left ventricle and of the middle right coronary artery at level 3 (Fig. 1c), and of the distal

right coronary artery at level 4 (Fig. 1d).

Comparison of aortic enhancement in the 2 BW groups

P1 and P2 patients were divided into lighter and heavier BW groups; we used 58 kg as the BW threshold because the mean weight of Japanese patients undergoing CM–enhanced CT was approximately 58 kg. We compared the contrast enhancement of the ascending aorta at level 1 obtained with both protocols in lighter and heavier patients.

Success rate of adequate vessel enhancement

Cademartiri et al. (6, 19) reported that greater intracoronary attenuation leads to higher diagnostic accuracy in the detection of coronary artery stenosis and improves the visualization of small coronary vessels at MDCT. They classified their patients into a low (287 ± 29 HU) and high (371 ± 39 HU) coronary attenuation group and found that sensitivity and specificity were greater in the high- than the low attenuation group. Based on their observations we selected an attenuation value of 300 HU or more to indicate adequate enhancement of the ascending aorta and compared P1 and P2 patients.

Image noise

We defined image noise as the SD of the attenuation values of the ascending aorta at level 1 and 2 (Fig. 1a, b) and as the SD of the septal myocardial wall at level 3 and 4 (Fig. 1c, d).

Qualitative CT Image Analysis

Two subspecialty radiologists (Y.Y. and K.A., with 4 and 5 years of experience, respectively) were blinded to the examination techniques, and they independently reviewed CT images. Each radiologist independently graded the images for beam-hardening artifacts (streak artifacts), image noise, vessel enhancements and diagnostic acceptability by using a three-point scale. Streak artifacts were graded on a three-point scale (1, streak artifacts absent; 2, streak artifacts present but not interfering with depiction of adjacent structures; 3, streak artifacts present and interfering with depiction of adjacent structures). The extent of "graininess" or "mottle" on the CT images was the main determinant in the grading of image noise. Image noise was graded on a three-point scale (1, acceptable; 2, average graininess was seen with satisfactory depiction of small

structures; 3, unacceptable). Diagnostic acceptability was graded on the basis of satisfactory depiction of coronary arteries, vessel wall and soft-tissue structures for diagnosis. Diagnostic acceptability was graded on a three-point scale (1, unacceptable; 2, acceptable; 3, excellent). Inter-observer disagreements were proved by consensus.

Statistical Analysis

All numeric values are reported as the mean ± SD. To compare the attenuation values and the image noise between P1 and P2, and to compare differences in aortic enhancement between the 2 BW groups treated by P1 or P2 we used the two-tailed Student *t*-test. The Fisher exact probability test was used for comparison of adequate vessel enhancement in the ascending aorta with P1 and P2. Differences of $p < 0.05$ were considered to be statistically significant. For statistical analyses we used a statistical software package (SPSS, version 15.0; SPSS, Chicago, IL, USA).

RESULTS

Attenuation values in each portion

Mean contrast density in the superior vena cava, right- and left ventricle, ascending aorta, left main coronary artery, and the proximal-, middle-, and distal segment of the right coronary artery CA is shown in Table 1. The attenuation values of the superior vena cava and the right and left ventricle were significantly higher in P1 than P2 ($p < 0.01$), however, there was no significant difference in the attenuation values of the ascending aorta, left main coronary artery, and the proximal-, middle-, and distal segment of the right coronary artery.

Comparison of aortic enhancement between the 2 BW groups (Fig. 2)

Under P1, mean aortic enhancement was 421.3 ± 51.5 HU in patients weighing less than 58 kg; it was 397.2 ± 42.3 HU in patients with a BW equal to- or more than 58 kg; the difference was statistically significant ($p = 0.03$). Under P2, these values were 407.6 ± 85.1 and 409.2 ± 47.9 HU

and the difference was not statistically significant ($p = 0.17$).

Representative coronal images of P1 and P2 patients of the higher or lower BW are shown in Fig. 3. Under P2, vessel enhancement on the left side of the heart was similar in both BW groups. On the other hand, under P1, better vessel enhancement was obtained in the lower- than the higher BW group.

Success rate of adequate vessel enhancement (Table 2)

Under P1, 25 of 30 patients (83.3%) satisfied the criteria for adequate enhancement of the ascending aorta. On the other hand, all P2 patients satisfied this requirement; the difference was statistically significant ($p = 0.03$).

Image Noise (Table 3)

As shown in Table 3, in P1 patients the image noise of the ascending aorta and of the myocardium was significantly higher than in P2 patients ($p < 0.05$).

Representative cases are shown in Fig. 4. Under P1, streak artifacts arising from dense CM in the superior vena cava resulted in image-quality degradation. On the other hand, P2 prevented CM "pooling" on the right side of the heart, this resulted in image noise abatement.

DISCUSSION

Because reported CM injection protocols for coronary CTA with 4- or 16-detector CT scanners were based on fixed injection rates, injection durations, and CM doses irrespective of the patient's body size (7-13), they may not be optimal for 64-detector CT scanners. Their shorter scan time makes it possible to decrease the injection duration and the CM dose at CTA (12). Earlier studies on optimal contrast injection protocols for coronary CTA (7, 13) pointed out that it was essential to achieve sufficient enhancement of the coronary arteries and to eliminate beam-hardening artifacts arising from dense CM within the right side of the heart. Our study showed that compared to conventional fixed-dose protocols, protocols with the contrast dose

tailored to the patient BW and a fixed short injection duration satisfy these requirements and reduce the average CM volume required for coronary CTA scans obtained with 64-detector CT scanners. Although P1 and P2 yielded comparable attenuation values at the coronary arteries and ascending aorta, with P2 the image noise of the ascending aorta at level 1 and 2 and of the myocardium at level 3 was significantly lower.

Although irrespective of patient BW, fixed CM doses are commonly used at cardiac CTA, we found that tailoring the contrast dose to the BW facilitated stable aortic enhancement at coronary CTA. There was no statistically significant difference between lighter and heavier P2 patients with respect to aortic enhancement. On the other hand, under P1, mean aortic enhancement was significantly lower in the higher- than the lower BW group. According to Fleischmann (20), in fixed-dose protocols the central blood volume is inversely correlated with arterial enhancement and correlated with BW. Protocols with CM doses tailored to BW and delivered at fixed injection durations have been shown to reduce inter-individual differences in arterial enhancement (15). Our results support these findings and suggest that protocols with BW-tailored CM doses and fixed injection durations can be used in patients undergoing coronary CTA.

P1 and P2 did not differ significantly with respect to attenuation of the ascending aorta and coronary arteries. This suggests that the 15-sec injection duration is adequate for coronary CTA using a 64-detector CT scanner and the bolus tracking technique. With P2, on the other hand, attenuation of the left ventricle was significantly lower than with P1, indicating that under P2, scanning continued after arterial peak enhancement at the level of the left ventricle to the ascending aorta. Therefore, in protocols with injection durations shorter than 15 sec and bolus tracking, arterial enhancement may decrease and become unstable.

Our protocol abates the beam-hardening artifact that arises from the right side of the heart. In clinical studies, an increase in the object size and density resulted in beam-hardening artifacts; in fact, dense CM in the superior vena cava and right ventricle was the leading cause of beam-hardening artifacts at cardiac CT (10, 13). Protocols with BW-tailored contrast doses and

fixed injection durations prevent CM "pooling" on the right side of the heart and eliminate image noise at levels 1 - 3. We found that the short injection duration and constant enhancement timing of BW-tailored protocols eliminated the image noise without a deterioration in the enhancement of the coronary arteries.

There were some potential limitations in our study. First, as the range and mean of our patients' body weight were smaller than in North American and European patients, the applicability of our results to non-Japanese populations must be assessed. Second, P1 and P2 differed with respect to the average CM dose and the injection duration and at present, we do not know whether these differences affected our results. Nonetheless, we suggest that protocols in which the CM dose is BW-tailored and the injection duration is fixed, can be used in patients undergoing coronary CTA. The shorter scan time of 64-detector CT scanners makes it possible to shorten the CM injection duration and we posit that a 15-sec injection duration is optimal for 64-row coronary CTA with bolus tracking.

In conclusion, we documented that protocols in which the CM dose is BW-tailored and the injection duration is short and fixed yielded adequate enhancement of the coronary arteries and ascending aorta, and eliminated the beam-hardening artifact arising from the right side of the heart that is encountered with conventional fixed-dose protocols.

Chapter III MDCT evaluation of myocardial bridging

Abstract

Objective-We evaluated the relationship between the myocardial bridging and focal coronary atherosclerosis using MDCT angiography (MD-CTA).

Background-Pathological reports suggested that wall shear-stress proximal to myocardial bridging results in focal coronary atherosclerosis. This hypothesis was not confirmed clinically.

Methods-We retrospectively reviewed the baseline characteristics of 130 patients and the results of coronary MD-CTA studies performed on a 40-detector row CT. The images were reviewed by 2 cardiac radiologists. We grouped the left anterior descending coronary artery (LAD) segments into complete-, incomplete-, and no myocardial bridging. The plaque burden in the proximal and middle segment of the LAD was scored as 0, no plaque; 1, small plaque; or 2, large plaque. Of the 130 LAD segments, 56 were classified as no-, 40 as incomplete-, and 34 as complete bridging. There was no statistically significant difference in the baseline characteristics among the 3 groups.

RESULTS-The mean visual scores for plaque burden in the proximal and middle segment of the LAD were 0.9 ± 0.9 and 0.6 ± 0.9 in the no bridging group, and 1.1 ± 0.9 and 0.2 ± 0.4, and 1.5 ± 0.7 and 0.1 ± 0.3 in the incomplete- and complete bridging group, respectively. Scores in the proximal LAD were significantly higher in the complete bridging- than the no-bridging group ($p<.05$). Scores in the middle LAD were significantly greater in the no- than the complete- and incomplete- bridging group ($p<.05$).

Conclusions-The segment proximal to the myocardial bridge frequently showed atherosclerotic plaque formation while the tunneled segment did not.

Introduction

Myocardial bridging is a congenital anomaly in which a segment of a coronary artery is surrounded by myocardium. The artery covered with myocardium is called a tunneled artery and myocardial bridging is most commonly found in the middle segment of the left anterior descending coronary artery (LAD) (1).

Myocardial bridging usually carries a benign prognosis, although some cases associated with myocardial ischemia, infarction, and sudden death have been reported(2-4). It has been suggested that myocardial bridging is associated with the development of atherosclerosis proximal to the tunneled artery in the LAD(5-8). However, due to limitations in the ability of catheter coronary angiography to detect myocardial bridges, their role as an independent factor in the development of atherosclerotic plaques has not been confirmed.

Recent advances in multi-detector CT (MDCT) facilitate the non-invasive assessment of the coronary artery and a preliminary report has shown that this technique can detect myocardial bridges, visualize the coronary artery lumen and wall, and allow for inspection of the surrounding myocardium and assessment for the presence or absence of atherosclerosis(9).

The purpose of this study was to clarify whether myocardial bridging has some relationship for progression of atherosclerotic plaque of the proximal segment of the LAD. We evaluated a series of MDCT coronary angiographs and the risk factors for arteriosclerosis.

Materials and Methods

Study Population

We retrospectively studied 142 patients with known or suspected coronary disease who underwent cardiac CT examination between December 2004 and December 2005 at our institute. We excluded 12 patients with tachycardia or arrhythmia (n=7), severe coronary artery calcification (n=4), and poorly enhanced coronary vessels (n=1) because the quality of the images was unacceptable. Thus, the study population consisted of 130 patients, 84 men and 46 women ranging in age from 18 to 89 years (mean 66.4 years). All patients who underwent cardiac CT examination at Kumamoto University Hospital, Kumamoto, Japan, gave prior informed consent for the use of their CT images in future retrospective studies. The Institutional Review board approved the use of the CT database and waived the requirement for informed specific study-related patient consent.

Scan Protocol and Image Reconstruction

Five minutes prior to scanning, each patient received 0.3 mg of nitroglycerin sublingually to dilate the coronary arteries. Beta-blockers were not administered to avoid the risk of anaphylactoid reaction from the radiographic contrast media(10, 11).

Using a 40–detector CT scanner (Brilliance-40; Philips Medical Systems, Ohio), contrast-enhanced MDCT examinations were performed with the patients in the supine position during a single breath-hold. The scanning protocol was as follows: collimation of 40 sections, individual section thickness 0.625 mm (40 x 0.625 mm), table feed increments 11.9 mm/sec, pitch 0.2, tube rotation time 420 msec, tube voltage 120 kV, tube current time-product 600 mAs. Depending on the cardiac dimensions, the scanning time varied from 10 to 15 sec.

We inserted a 20-gauge i.v. catheter into an antecubital vein and using a power injector (Autoenhance A-250; Nemoto-Kyorindo, Tokyo, Japan), we injected 80 ml iopamidol (Iopamiron-370; Nihon Schering, Osaka, Japan) at a flow rate of 4 ml/s; this was followed by a chaser bolus of 20 ml saline solution at a flow rate of 4 ml/sec.

Computer-assisted bolus tracking technique was used to synchronize the arrival of the contrast medium in the coronary arteries with start of the scan(12). To monitor the arrival of the contrast material, at 8 sec after the start of contrast injection, we performed axial scans at the level of the ascending aorta. Scanning started automatically 6 sec after contrast enhancement reached 150 Hounsfield units in a region of interest in the ascending aorta.

Images were reconstructed with ECG gating to obtain an optimal, motion-free image quality; the z-axis resolution was 0.8 mm, the increments were 0.4 mm. Initially, a single data-set was reconstructed during the mid-diastolic phase (75% of the R-R interval). In cases with unsatisfactory image quality, image reconstruction of the raw data was performed at 0-, 10-, 20-, 30-, 40-, 50-, 60-, 70-, 80-, and 90% of the R-wave to R-wave interval to improve the image quality of all available coronary segments. We used a conventional single-sector algorithm when the heart rate was slower than 65 beats per minute (bpm) and a segmented cardiac reconstruction algorithm when it was faster than 66 bpm.

CT Image Evaluation

Image analysis was performed with multiplanar reformation (MPR), maximum intensity projection, volume rendering, and curved MPR (CPR); the images were transverse source images displayed on a computer workstation (ZIO M900, Zio Software, Tokyo, Japan).

We classified the middle coronary segments of the LAD into complete-, incomplete-, and no myocardial bridging groups. As others(6, 13, 14) suggested that superficial myocardial bridges were of low clinical significance and as the contrast and spatial resolution of MDCT made it difficult to distinguish between a thin myocardial bridge and the coronary arterial wall, we defined incomplete myocardial bridging as an intermediate grade. Myocardial bridging was classified as complete or incomplete based on the thickness of the overlying soft tissue; the thickness threshold was 1.5 mm (Fig. 1). All images were evaluated on imaging planes parallel and transverse section to the coronary artery.

The plaque burden in the proximal and middle coronary segment of the LAD was assessed

by the size of existing plaques. Plaques were classified as small or large based on visual inspection; the threshold for luminal decrease was 50%.

Two board-certified radiologists (T.N. and D.U.) with 4 and 6 years of experience interpreting cardiac CT independently evaluated the coronary MD-CTA. Both were blinded to clinical information on the patients.

Statistical Analysis

The baseline characteristics (age, sex, BMI, diabetes, hypertension, hyperlipidemia, and smoking history) of the patients were was compared using the Chi-square and The Kruskal-Wallis test.

Visual scores for plaque burden were compared among the patients using the Kruskal-Wallis test. If there was a statistically significant difference among the groups, pair-wise comparisons were performed with the Steel-Dwass test.

Interobserver agreement was measured with the Cohen Kappa test. The scale for the Kappa coefficients for interobserver agreement was: less than 0.20, poor; 0.21–0.40, fair; 0.41–0.60, moderate; 0.61–0.80, substantial; and 0.81–1.00, almost perfect(15, 16).

Statistical analyses were performed with commercially available software (SPSS, version 10.05; SPSS, Chicago, IL); differences of $p<.05$ were considered statistically significant.

RESULTS

Baseline Patient Characteristics

Table 1 summarizes the baseline characteristics of the 130 patients and the incidence of no myocardial bridging and of complete- and incomplete bridging. Of the 130 patients, 56 had no myocardial bridges; 40 had incomplete- and 34 had complete myocardial bridges. There were no significant differences in the baseline characteristics except for gender; of the 34 patients with complete myocardial bridging, 28 were males ($p<.05$).

Plaque Burden in the Proximal Segment of the LAD

The grade assigned by visual inspection for plaque burden in the proximal segment of the LAD is shown in Table 2. The mean visual scores were 0.9 ± 0.9 for the no bridging group, 1.1 ± 0.9 for the incomplete-, and 1.5 ± 0.7 for the complete bridging group. The scores for plaque burden were significantly higher in the complete- than the no bridging group ($p<.05$). There was no statistically significant difference in the scores for the other pairs.

There was substantial interobserver agreement with respect to the plaque burden in the proximal segment of the LAD (Kappa = 0.67).

Plaque Burden in the Middle Segment of the LAD

The visual grades assigned for plaque burden in the proximal segment of the LAD are shown in Table 3. The mean visual scores were 0.6 ± 0.9 for the no bridging group, 0.2 ± 0.4 for the incomplete- and 0.1 ± 0.3 for the complete bridging group. The scores assigned for plaque burden were significantly higher in the complete- and incomplete bridging group than in patients with no myocardial bridging ($p<.05$). There was no significant difference in the scores for the other pairs.

There was substantial interobserver agreement with respect to the plaque burden in the proximal segment of the LAD (Kappa = 0.61).

Illustrative Case

This 62-year-old man suffered repeated episodes of chest pain. Exercise ECG and myocardial perfusion SPECT were suspicious for an old anterior myocardial infarction with ischemia. Conventional coronary angiography showed a large intraluminal filling defect and a distal 'milking effect' in the LAD (Figs. 2A, 2B). MDCT coronary angiography showed complete myocardial bridging in the middle segment of the LAD and a large plaque just proximal to the tunneled artery (Figs. 2C, 2D). MDCT yielded precise information on the location, length and depth of the myocardial bridge and the atherosclerotic status.

DISCUSSION

As myocardial bridging is a common autopsy finding in normal subjects, its clinical significance remains controversial. It has been considered a benign condition; coronary narrowing occurs during systole and most coronary flow is during diastole. However, some patients with myocardial bridging suffered myocardial ischemia, infarction, and sudden death(2-4) and there appears to be an association between myocardial bridging and acute anterior wall myocardial infarction due to stenosis or occlusion of the LAD(17, 18). Our study clarified that myocardial bridging is a significant independent factor for arteriosclerosis proximal to and in the tunneled artery.

A connection between intimal arteriosclerosis and myocardial bridging is supported by findings made on the cellular and ultrastructural level(8, 19, 20). While present in the proximal and distal segments, foam cells and modified smooth muscle cells were absent in the tunneled segments(8). Cholesterol-fed rabbits developed intimal atherosclerosis in the extramural epicardial- but not the tunneled segment(19). These changes may be attributable to hemodynamic forces, i.e. low shear-stress at the entrance to- and high shear-stress in the tunneled segment(8, 19, 20). Low shear-stress in the area proximal to the tunneled segment may induce the release of endothelial vasoactive agents such as endothelial nitric oxide synthase (eNOS), angiotensin-converting enzyme (ACE) (21), and endothelin-1 (ET-1), which participates in the pathogenesis of atherosclerosis at all stages, even when the plaque is clinically imperceptible(22).

Ge et al. reported atherosclerosis associated with myocardial bridging on the clinical level(23). When they performed intracoronary- and Doppler ultrasound in 14 patients with angiographic evidence of the 'milking effect' in the LAD, they found atherosclerotic plaques in the segments proximal to the bridge in 12 of their 14 patients. Because intravascular pressure was highest just proximal to the bridge and higher than aortic pressure, they concluded that blood flow disturbance and high wall stress proximal to the myocardial bridge were main contributors to the development of atherosclerosis in the segment proximal to the bridge.[5]

Although earlier reports suggested that myocardial bridging is associated with the

development of atherosclerosis proximal to the tunneled artery, to date, none provided evidence for myocardial bridging as an independent factor. Kramer et al.(24) and Juilliere et al.(25) reviewed large series of coronary angiographs to assess the clinical importance of myocardial bridging; they reported that most patients with 'milking effect' had a good prognosis. However, we postulate that limitations of catheter coronary angiography render this conclusion uncertain. Angiographically, due to coronary narrowing during systole, myocardial bridging is characterized by a 'milking effect' (26). Although this effect is considered diagnostic, in autopsy and coronary angiographic series, the incidence of myocardial bridging ranged from 15 to 85%(7, 13, 27, 28) and from 0.5% to 2.5%, (24-26, 29) respectively. We suggest that the low angiographic prevalence rate can be explained by minimal or no compression by thin bridges, or the presence of an atherosclerotic lesion resulting in physiologic stenosis proximal to the bridge(30).

MDCT coronary angiography offers advantages over coronary angiography for the evaluation of myocardial bridging because it is a noninvasive imaging modality that allows assessment of the coronary artery lumen, wall, and surrounding myocardium(1, 9). In addition, it yields information on the length, depth, and precise location of atherosclerosis associated with myocardial bridging. In our preliminary study we found that patients with complete myocardial bridging on MDCT frequently developed intimal atherosclerosis in the proximal segment of the LAD without involvement of the tunneled segment.

The present study has some limitations. We cannot rule out a population bias because our series was confined to patients with suspected or confirmed ischemic heart disease. We excluded patients who manifested an unstable sinus rhythm or a relatively fast heart rate because these variables degrade the quality of the MDCT images. Although different findings may be obtained in low-risk and asymptomatic patients, our series reflects the population encountered in the clinical context. We also did not perform a comparison study between pathological- and MDCT coronary angiographic findings, however, the excellent diagnostic performance of MDCT coronary angiography in the detection of coronary plaques has been documented(31-33).

Our current results were based on the analysis of studies performed at a single center.

We are in the process of performing multicenter studies to further assess the clinical significance of myocardial bridging.

Conclusion

Myocardial bridging is a common finding on MDCT coronary angiographs. The segment proximal to the bridge is frequently involved in atherosclerotic plaque formation with sparing of the tunneled segment.

General conclusion

In this report, we studied about the optimal view of fusion imaging, optimal contrast injection protocol for coronary CTA using 64-row MSCT, and the incidence and clinical significance of myocardial bridging on cardiac CT.

First, 3D volume-rendering fused images of coronary CT angiography and myocardial SPECT present a panoramic view of the coronary vessels and myocardial perfusion, the relationship between the diseased artery and the myocardium can be determined without requiring difficult mental integration by the evaluator.

Second, our results revealed that contrast injection protocol with a dose tailored with patient body weight and fixed short injection duration provide almost constant adequate enhancement of the coronary arteries and ascending aorta, and the abatement of the beam-hardening artifact arising from the right side of heart as compared with conventional fixed dose protocol.

Lastly, myocardial bridging is a common finding on MDCT coronary angiographs. The segment proximal to the bridge is frequently involved in atherosclerotic plaque formation with sparing of the tunneled segment.

Many reports suggest that MSCT is a highly accurate tool for the non-invasive detection of coronary artery disease. But further technical advances are expected in acquisition techniques and post-processing of the CT data.

References – chapter I

1. Schindler TH, Magosaki N, Jeserich M, et al. Fusion imaging: combined visualization of 3D reconstructed coronary artery tree and 3D myocardial scintigraphic image in coronary artery disease. Int J Card Imaging. 1999;15:357-368.

2. Schindler, TH, Magosaki N, Jeserich M, et al. 3D Assessment of myocardial perfusion parameter combined with 3D reconstructed coronary artery tree from digital coronary angiograms. Int J Card Imaging. 2000;16:1-12.

3. Faber TL, Santana CA, Garcia EV, et al. Three-dimensional fusion of coronary arteries with myocardial perfusion distributions: clinical validation. J Nucl Med. 2004;45:745-753.

References – chapter II

1. Leber AW, Becker A, Knez A, et al. Accuracy of 64-slice computed tomography to classify and quantify plaque volumes in the proximal coronary system: A comparative study using intravascular ultrasound. J Am Coll Cardiol 2006; 47:672-677.
2. Maintz D, Seifarth H, Raupach R, et al. 64-slice multidetector coronary CT angiography: In vitro evaluation of 68 different stents. Eur Radiol 2006; 16:818-826.
3. Nishino M, Kubo T, Kataoka ML, Raptopoulos V, Hatabu H. Coronal reformations of the chest on 64-row multi-detector row CT: Evaluation of image quality in comparison with 16-, 8- and 4-row multi-detector row CT. Eur J Radiol 2006; 59:231-237.
4. Pannu HK, Jacobs JE, Lai S, Fishman EK. Coronary CT angiography with 64-MDCT: Assessment of vessel visibility. AJR Am J Roentgenol 2006; 187:119-126.
5. Rixe J, Achenbach S, Ropers D, et al. Assessment of coronary artery stent restenosis by 64-slice multi-detector computed tomography. Eur Heart J 2006; 27:2567-2572.
6. Cademartiri F, Mollet NR, Lemos PA, et al. Higher intracoronary attenuation improves diagnostic accuracy in MDCT coronary angiography. AJR Am J Roentgenol 2006; 187:W430-433.
7. Utsunomiya D, Awai K, Sakamoto T, et al. Cardiac 16-MDCT for anatomic and functional analysis: Assessment of a biphasic contrast injection protocol. AJR Am J Roentgenol 2006; 187:638-644.
8. Rist C, Nikolaou K, Kirchin MA, et al. Contrast bolus optimization for cardiac 16-slice computed tomography: Comparison of contrast medium formulations containing 300 and 400 milligrams of iodine per milliliter. Invest Radiol 2006; 41:460-467.
9. Cademartiri F, Nieman K, van der Lugt A, et al. Intravenous contrast material administration at 16-detector row helical CT coronary angiography: Test bolus versus bolus-tracking technique. Radiology 2004; 233:817-823.
10. Cademartiri F, Mollet N, van der Lugt A, et al. Non-invasive 16-row multislice CT coronary

angiography: Usefulness of saline chaser. Eur Radiol 2004; 14:178-183.

11. Cademartiri F, de Monye C, Pugliese F, et al. High iodine concentration contrast material for noninvasive multislice computed tomography coronary angiography: Iopromide 370 versus iomeprol 400. Invest Radiol 2006; 41:349-353.

12. Funabashi N, Suzuki K, Terao M, et al. New acquisition method to exclusively enhance the left side of the heart by a small amount of contrast material achieved by multislice computed tomography with 64 data acquisition system. Int J Cardiol 2006.

13. Becker CR, Hong C, Knez A, et al. Optimal contrast application for cardiac 4-detector-row computed tomography. Invest Radiol 2003; 38:690-694.

14. Utsunomiya D, Awai K, Tamura Y, et al. 16-MDCT aortography with a low-dose contrast material protocol. AJR Am J Roentgenol 2006; 186:374-378.

15. Awai K, Hiraishi K, Hori S. Effect of contrast material injection duration and rate on aortic peak time and peak enhancement at dynamic CT involving injection protocol with dose tailored to patient weight. Radiology 2004; 230:142-150.

16. Awai K, Hori S. Effect of contrast injection protocol with dose tailored to patient weight and fixed injection duration on aortic and hepatic enhancement at multidetector-row helical CT. Eur Radiol 2003; 13:2155-2160.

17. Nakayama Y, Awai K, Funama Y, et al. Lower tube voltage reduces contrast material and radiation doses on 16-MDCT aortography. AJR Am J Roentgenol 2006; 187:W490-497.

18. Sandstede JJ, Tschammler A, Beer M, Vogelsang C, Wittenberg G, Hahn D. Optimization of automatic bolus tracking for timing of the arterial phase of helical liver CT. Eur Radiol 2001; 11:1396-1400.

19. Cademartiri F, Mollet NR, van der Lugt A, et al. Intravenous contrast material administration at helical 16-detector row CT coronary angiography: Effect of iodine concentration on vascular attenuation. Radiology 2005; 236:661-665.

20. Fleischmann D. High-concentration contrast media in MDCT angiography: Principles and rationale. Eur Radiol 2003; 13 Suppl 3:N39-43.

References – chapter III

1. Mohlenkamp S, Hort W, Ge J, Erbel R. Update on myocardial bridging. In:Circulation, 2002; 2616-2622.
2. Bestetti RB, Costa RS, Zucolotto S, Oliveira JS. Fatal outcome associated with autopsy proven myocardial bridging of the left anterior descending coronary artery. Eur Heart J 1989; 10:573-576.
3. Tio RA, Van Gelder IC, Boonstra PW, Crijns HJ. Myocardial bridging in a survivor of sudden cardiac near-death: role of intracoronary doppler flow measurements and angiography during dobutamine stress in the clinical evaluation. Heart 1997; 77:280-282.
4. Cutler D, Wallace JM. Myocardial bridging in a young patient with sudden death. Clin Cardiol 1997; 20:581-583.
5. Ge J, Erbel R, Gorge G, Haude M, Meyer J. High wall shear stress proximal to myocardial bridging and atherosclerosis: intracoronary ultrasound and pressure measurements. In:Br Heart J, 1995; 462-465.
6. Ishikawa Y, Akasaka Y, Ito K, et al. Significance of anatomical properties of myocardial bridge on atherosclerosis evolution in the left anterior descending coronary artery. Atherosclerosis 2006; 186:380-389.
7. Ishii T, Hosoda Y, Osaka T, et al. The significance of myocardial bridge upon atherosclerosis in the left anterior descending coronary artery. J Pathol 1986; 148:279-291.
8. Ishii T, Asuwa N, Masuda S, Ishikawa Y. The effects of a myocardial bridge on coronary atherosclerosis and ischaemia. J Pathol 1998; 185:4-9.
9. Goitein O, Lacomis JM. Myocardial bridging: noninvasive diagnosis with multidetector CT. In:J Comput Assist Tomogr, 2005; 238-240.
10. Lang DM, Alpern MB, Visintainer PF, Smith ST. Increased risk for anaphylactoid reaction from contrast media in patients on beta-adrenergic blockers or with asthma. Ann Intern Med 1991; 115:270-276.
11. Javeed N, Javeed H, Javeed S, Moussa G, Wong P, Rezai F. Refractory anaphylactoid shock potentiated by beta-blockers. Cathet Cardiovasc Diagn 1996; 39:383-384.
12. Sandstede JJ, Tschammler A, Beer M, Vogelsang C, Wittenberg G, Hahn D. Optimization of automatic bolus tracking for timing of the arterial phase of helical liver CT. Eur Radiol 2001; 11:1396-1400.
13. Ferreira AG, Jr., Trotter SE, Konig B, Jr., Decourt LV, Fox K, Olsen EG. Myocardial bridges: morphological and functional aspects. Br Heart J 1991; 66:364-367.
14. Ge J, Jeremias A, Rupp A, et al. New signs characteristic of myocardial bridging demonstrated by intracoronary ultrasound and Doppler. In:Eur Heart J, 1999; 1707-1716.
15. Landis JR, Koch GG. The measurement of observer agreement for categorical data. Biometrics 1977; 33:159-174.

16. Svanholm H, Starklint H, Gundersen HJ, Fabricius J, Barlebo H, Olsen S. Reproducibility of histomorphologic diagnoses with special reference to the kappa statistic. Apmis 1989; 97:689-698.

17. Schunkert H. Images in cardiovascular medicine. Focal coronary atherosclerosis proximal to myocardial bridging. In:Circulation, 2003; 1944.

18. Bauters C, Chmait A, Tricot O, Lamblin N, Van Belle E, Lablanche JM. Images in cardiovascular medicine. Coronary thrombosis and myocardial bridging. In:Circulation, 2002; 130.

19. Ishikawa Y, Ishii T, Asuwa N, Masuda S. Absence of atherosclerosis evolution in the coronary arterial segment covered by myocardial tissue in cholesterol-fed rabbits. Virchows Arch 1997; 430:163-171.

20. Masuda T, Ishikawa Y, Akasaka Y, Itoh K, Kiguchi H, Ishii T. The effect of myocardial bridging of the coronary artery on vasoactive agents and atherosclerosis localization. In:J Pathol, 2001; 408-414.

21. Malek AM, Alper SL, Izumo S. Hemodynamic shear stress and its role in atherosclerosis. Jama 1999; 282:2035-2042.

22. Ihling C, Szombathy T, Bohrmann B, Brockhaus M, Schaefer HE, Loeffler BM. Coexpression of endothelin-converting enzyme-1 and endothelin-1 in different stages of human atherosclerosis. Circulation 2001; 104:864-869.

23. Ge J, Erbel R, Rupprecht HJ, et al. Comparison of intravascular ultrasound and angiography in the assessment of myocardial bridging. In:Circulation, 1994; 1725-1732.

24. Kramer JR, Kitazume H, Proudfit WL, Sones FM, Jr. Clinical significance of isolated coronary bridges: benign and frequent condition involving the left anterior descending artery. Am Heart J 1982; 103:283-288.

25. Juilliere Y, Berder V, Suty-Selton C, Buffet P, Danchin N, Cherrier F. Isolated myocardial bridges with angiographic milking of the left anterior descending coronary artery: a long-term follow-up study. Am Heart J 1995; 129:663-665.

26. Noble J, Bourassa MG, Petitclerc R, Dyrda I. Myocardial bridging and milking effect of the left anterior descending coronary artery: normal variant or obstruction? In:Am J Cardiol, 1976; 993-999.

27. Polacek P, Kralove H. Relation of myocardial bridges and loops on the coronary arteries to coronary occulsions. In:Am Heart J, 1961; 44-52.

28. Hansen BF. Myocardial covering on epicardial coronary arteries. Prevalence, localization and significance. Scand J Thorac Cardiovasc Surg 1982; 16:151-155.

29. Angelini P, Trivellato M, Donis J, Leachman RD. Myocardial bridges: a review. Prog Cardiovasc Dis 1983; 26:75-88.

30. Bauters C, Chmait A, Tricot O, Lamblin N, Van Belle E, Lablanche JM. Images in cardiovascular medicine. Coronary thrombosis and myocardial bridging. Circulation 2002; 105:130.

31. Mollet NR, Cademartiri F, Nieman K, et al. Noninvasive assessment of coronary plaque burden using multislice computed tomography. Am J Cardiol 2005; 95:1165-1169.

32. Achenbach S, Moselewski F, Ropers D, et al. Detection of calcified and noncalcified coronary atherosclerotic plaque by contrast-enhanced, submillimeter multidetector spiral computed tomography: a segment-based comparison with intravascular ultrasound. Circulation 2004; 109:14-17.

33. Leber AW, Knez A, Becker A, et al. Accuracy of multidetector spiral computed tomography in identifying and differentiating the composition of coronary atherosclerotic plaques: a comparative study with intracoronary ultrasound. J Am Coll Cardiol 2004; 43:1241-1247.

Figure Legends - Chapter I-1

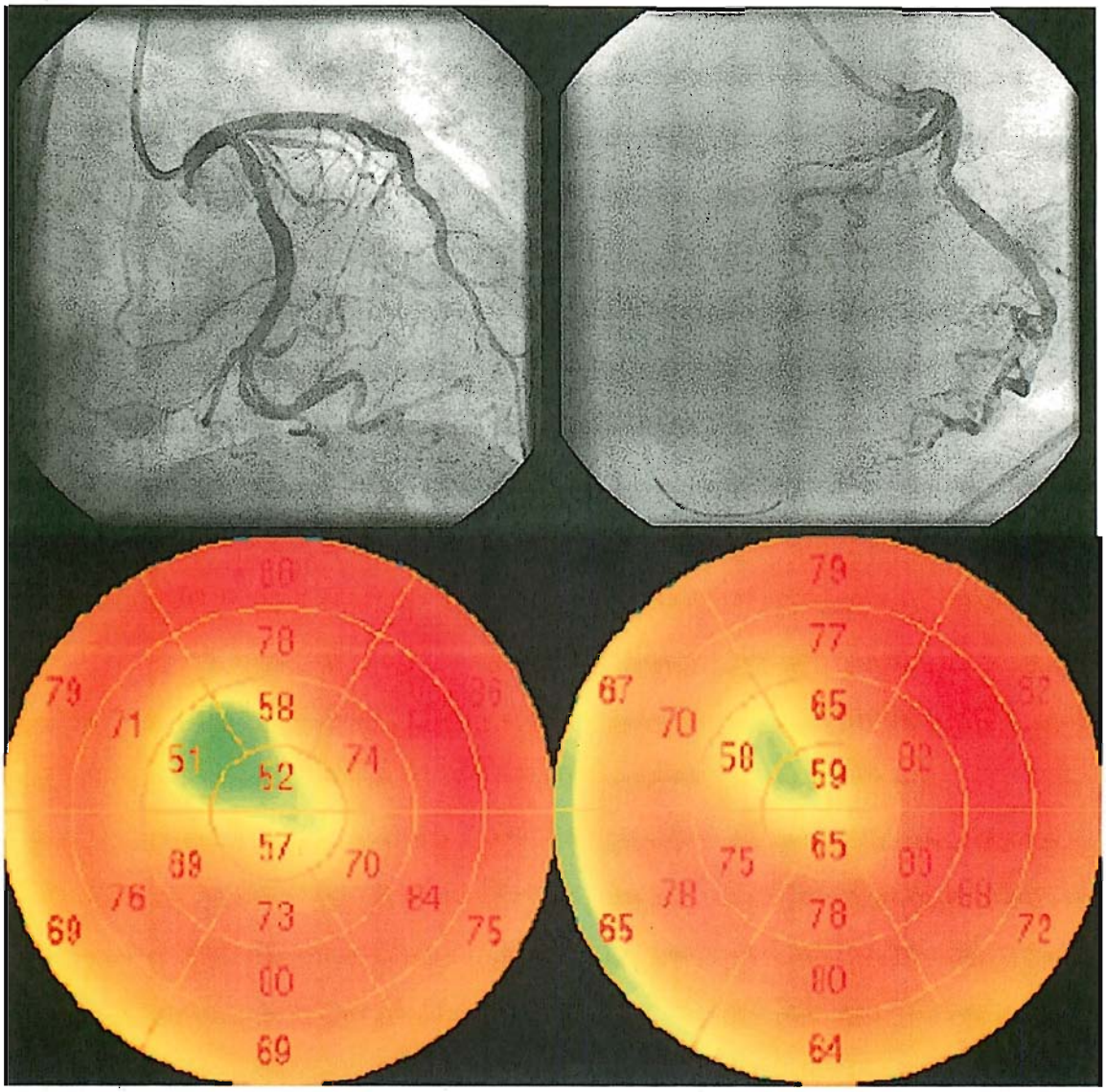

Figure 1 Conventional angiography and myocardial SPECT.

A 68-year-old woman with an acute myocardial infarction with left anterior descending artery stenosis had undergone percutaneous transluminal coronary angioplasty and coronary stenting. The coronary angiogram revealed 99% stenosis in the left anterior descending artery (LAD). Myocardial SPECT showed perfusion defect in the LAD territory with reverse redistribution.

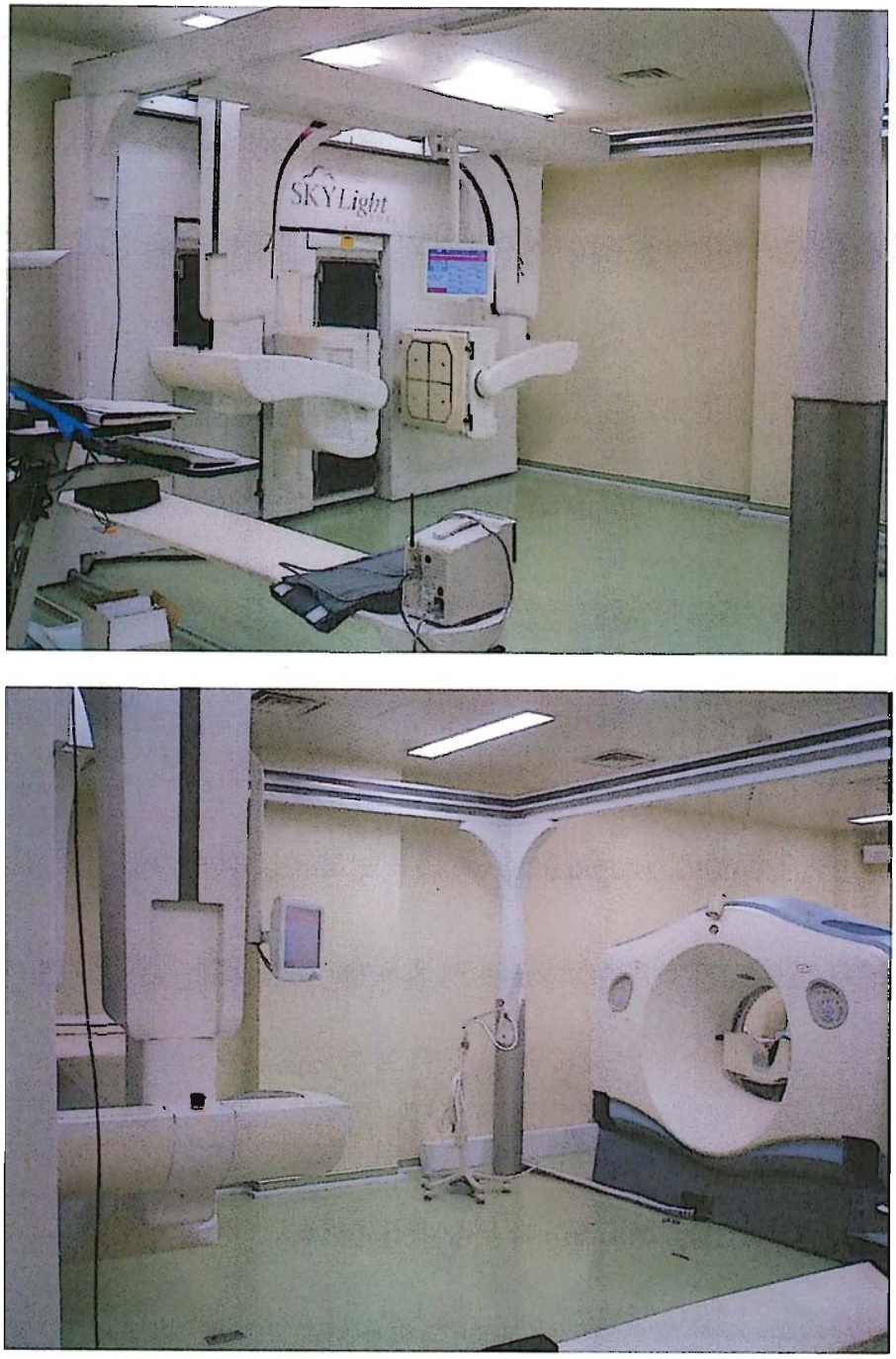

Figure 2. SPECT/CT combined system. 2-head ganmma camera (Skylight, ADAC, Milpitas, CA) and 8 -detector-row MDCT (Lightspeed ultra, GE, Milwaukee, WIis).

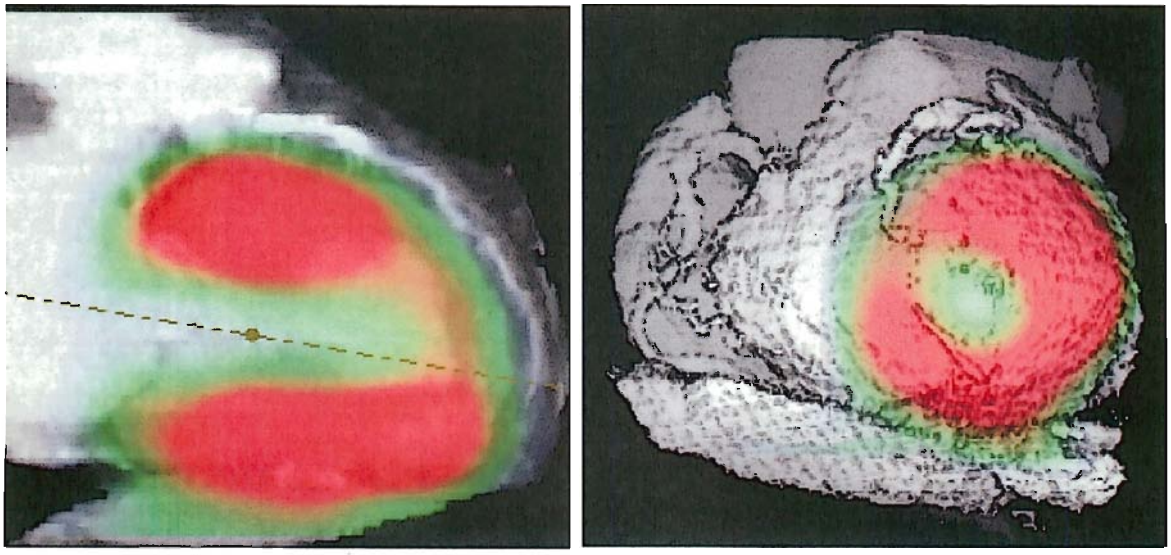

MPR Ray-Sum

Figure 3.Colored Ray-Sum and MPR image produced by original programs written in the Borland Delphi computer language.

MPR image clearly revealed the relationship between the myocardial perfusion defect and LAD. But, this method requires manual interpretation and mental integration of many images by the reviewer.

In Ray-Sum image, the relationship between the myocardial perfusion defect and coronary artery was unclear.

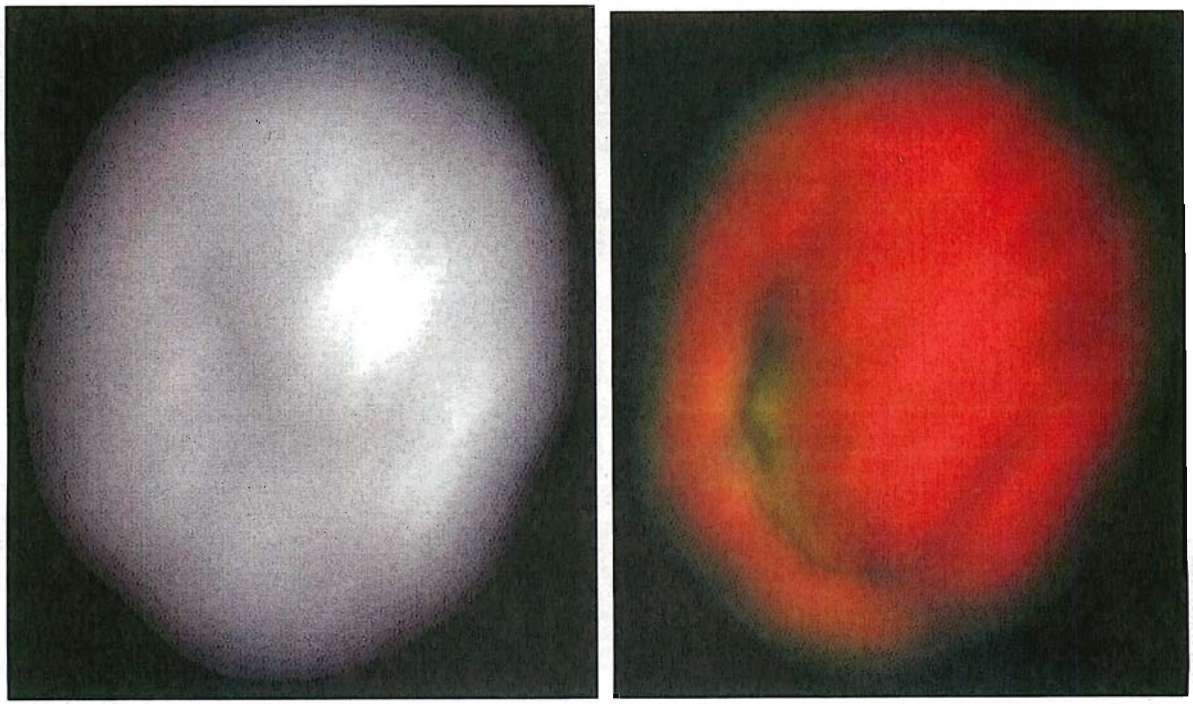

MIP image VR image

Figure 4 MIP and VR image reconstructed by CT workstation.

VR image clearly showed a perfusion defect in the anterior and septal wall as compared. On the other hand, myocardial perfusion defect is unclear in MIP image.

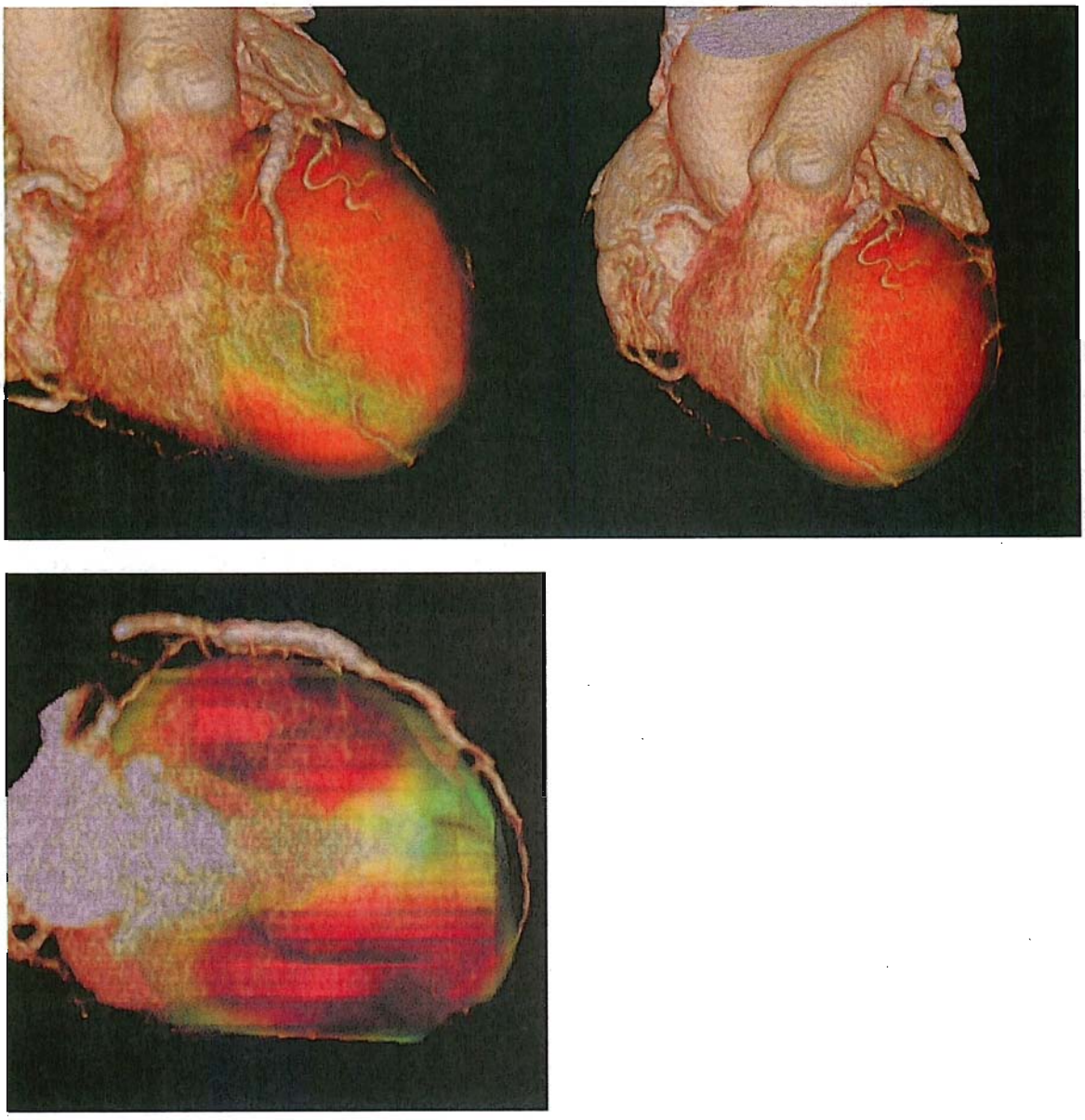

Figure 5 the 3D-volume rendering view showed a perfect match between the left anterior descending artery territory and the defect of tracer uptake

Figure Legends - Chapter I-2

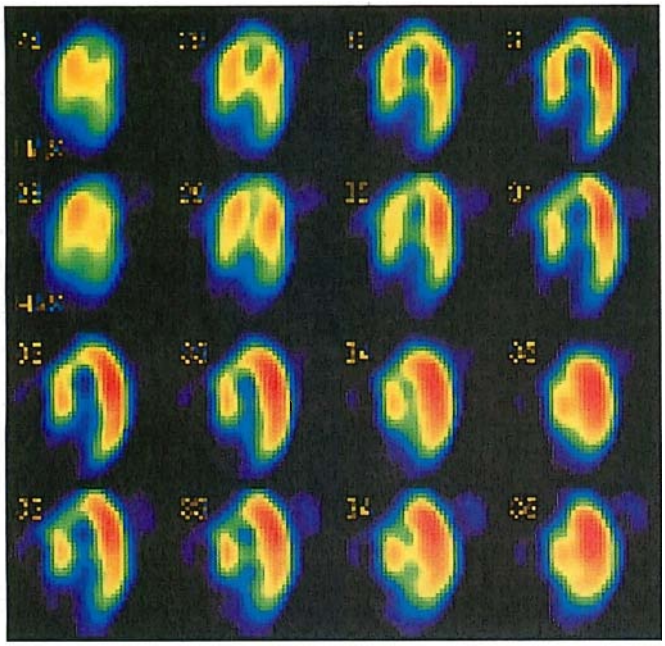

Fig 1a

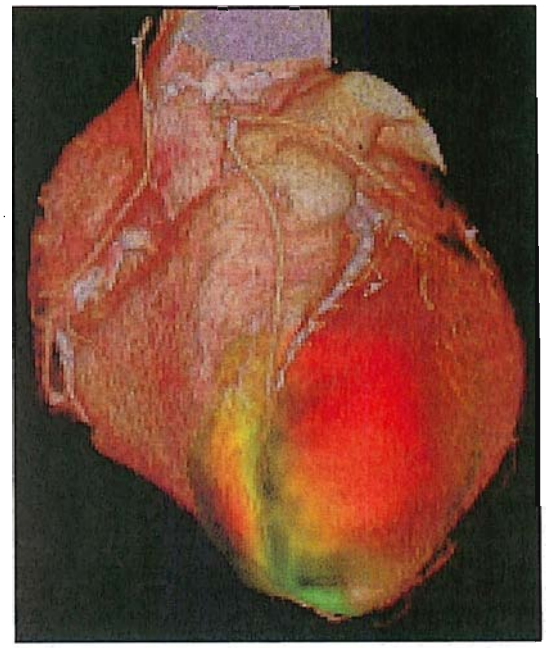

Fig 1b

Fig. 1.

A 62-year-old man who underwent coronary artery bypass grafting.

A. Myocardial perfusion SPECT (horizontal long-axis images). Stress images in the 1st and 3rd panel show a perfusion defect in the anterior and septal wall (small arrow). The redistribution images in the 2nd and 4th panel show reverse redistribution.

B. Volume-rendering fused images. The patency of the LITA-to-LAD bypass graft and the myocardial perfusion defect around the LAD are clearly depicted (arrow).

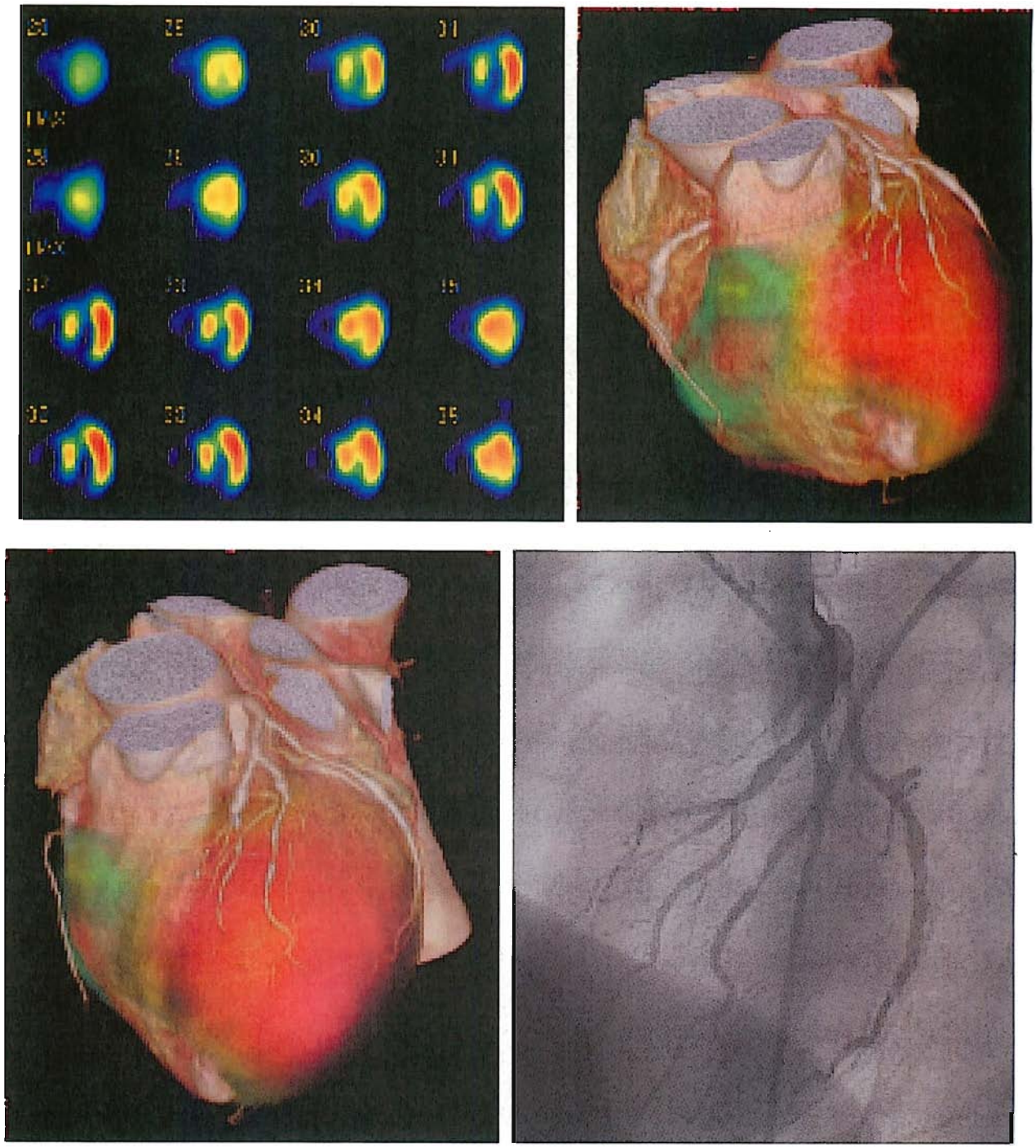

Figure 2. An 80-year-old man suspected old myocardial infarction with angina.

A. Myocardial perfusion SPECT (horizontal long-axis image) shows a perfusion defect in the anterior and septal wall with partial redistribution (small arrow). B, C. Volume-rendering fused images demonstrated a myocardial perfusion defect (B, small arrow) distal to the occluded coronary artery (seg.7, arrow) and a stenosed coronary artery (seg.9, small arrow). D. Conventional angiography showed occlusion of seg.7 (arrow) and 90% stenosis of seg.9 (small arrow).

Figure Legends - Chapter II-1

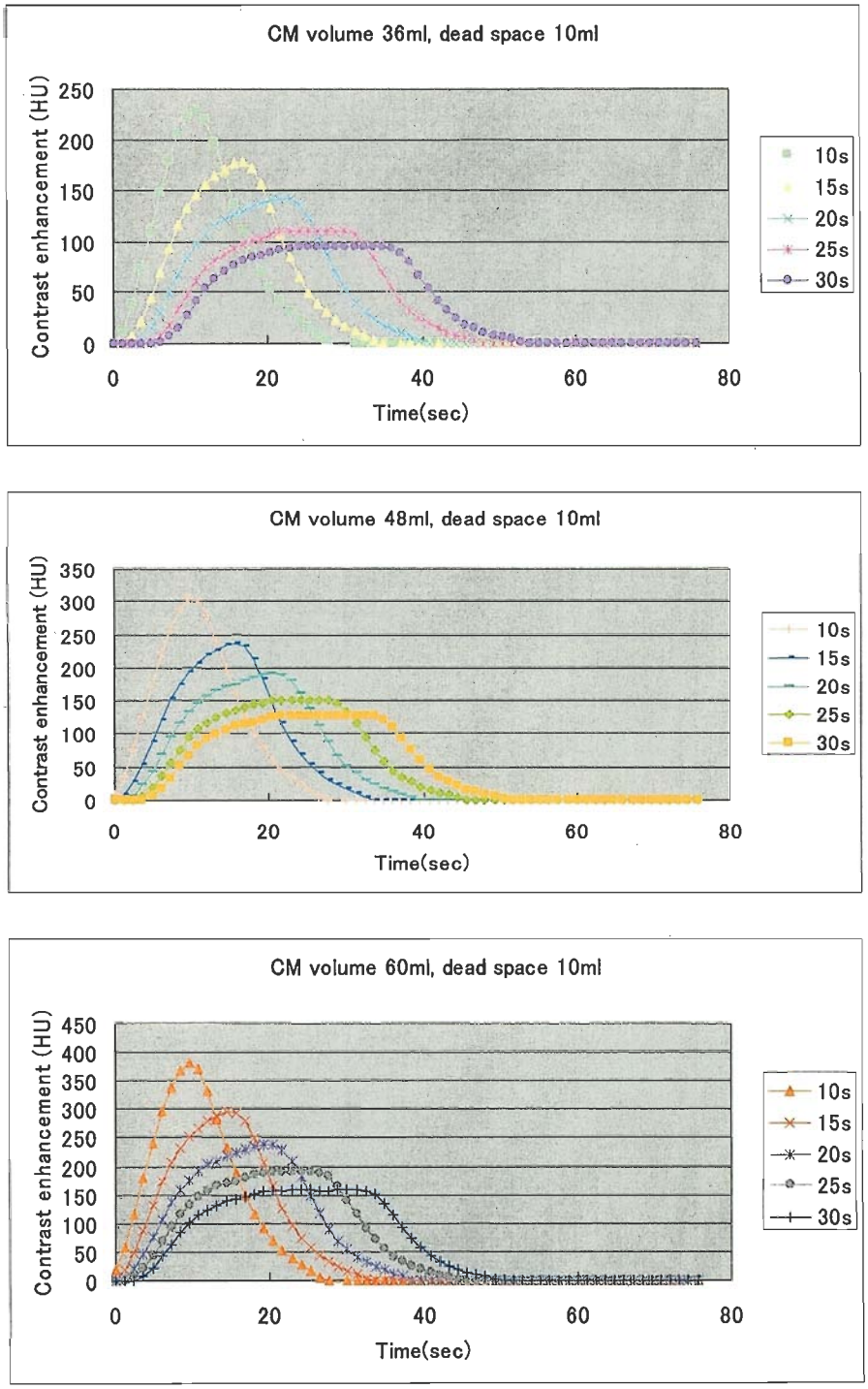

Figure 1. the average time–density curves with various contrast injection protocols.

Figure Legends - Chapter II-2

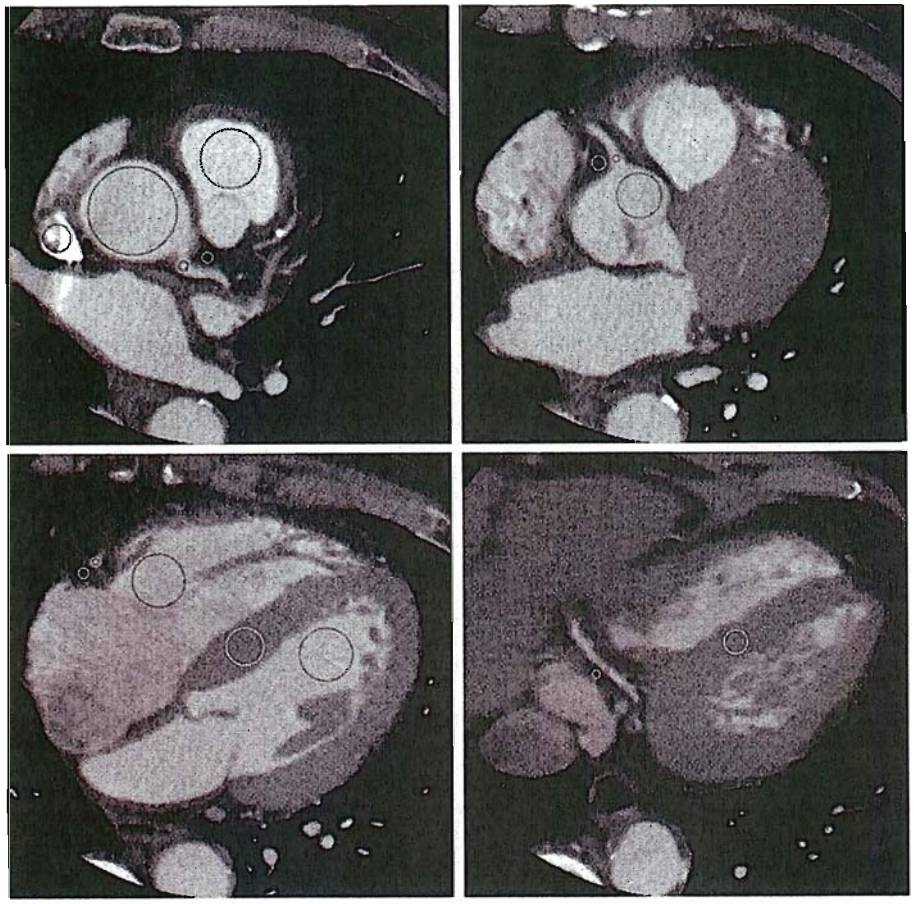

Figure 1: Examples of the 4 selected slices and regions of interest

Multi-detector row CT scans showing the 4 representative slice levels used in each patient for image evaluation. Top left: origin of the left main trunk. Top right: origin of the right coronary artery. Bottom left: center of the left ventricular cavity. Bottom right: bifurcation of the atrioventricular node branch.

Table 1 Attenuation values in each portion

Portion	Protocol 1 (HU)	Protocol 2 (HU)	P value
SVC	510.5±425.5	149.8±53.1	< 0.01
PA	398.2±186.1	138.6±53.1	< 0.01
RV	239.8±97.0	111.9±20.4	< 0.01
LV	415.7±89.4	309.9±79.2	< 0.01
Aorta	407.6±85.1	409.2±47.9	0.92
LM	380.7±90.5	384.2±51.9	0.85
proximal-RCA	398.2±93.9	374.1±52.8	0.22
middle-RCA	387.2±85.0	358.0±83.2	0.19
distal-RCA	370.0±97.0	337.0±72.7	0.14

Abbreviations

SVC: superior vena cava, PA: pulmonary artery trunk, RV: right ventricle, LV: left ventricle. LM: left main coronary artery, RCA: right coronary artery

* Data are the mean ± standard error.

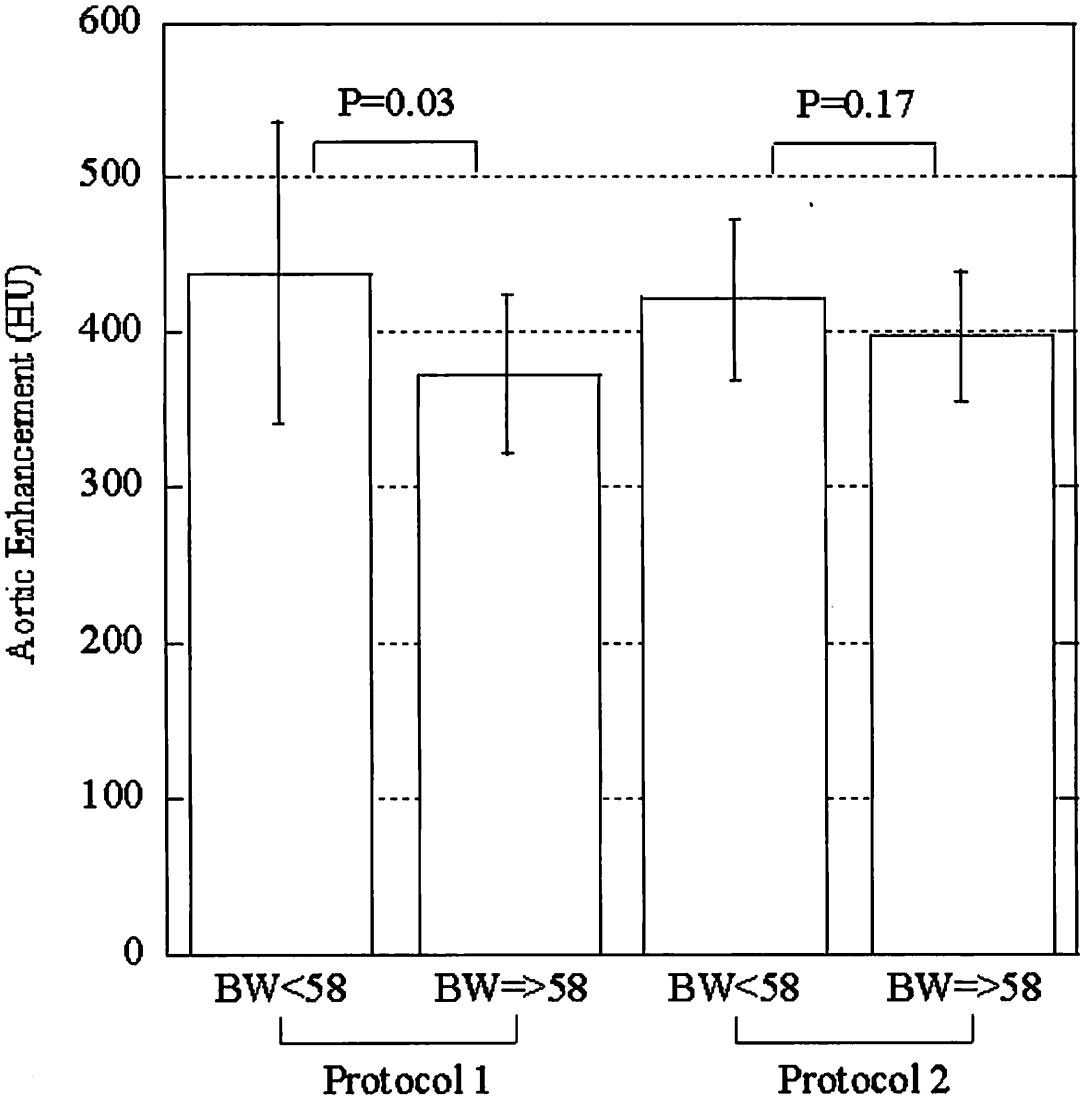

Figure 2: Graph of mean aortic attenuation obtained with the 2 protocols in the 2 body-weight groups.

(*)Under protocol 1, there was a statistically significant difference in mean attenuation between the high- and low-body weight groups.

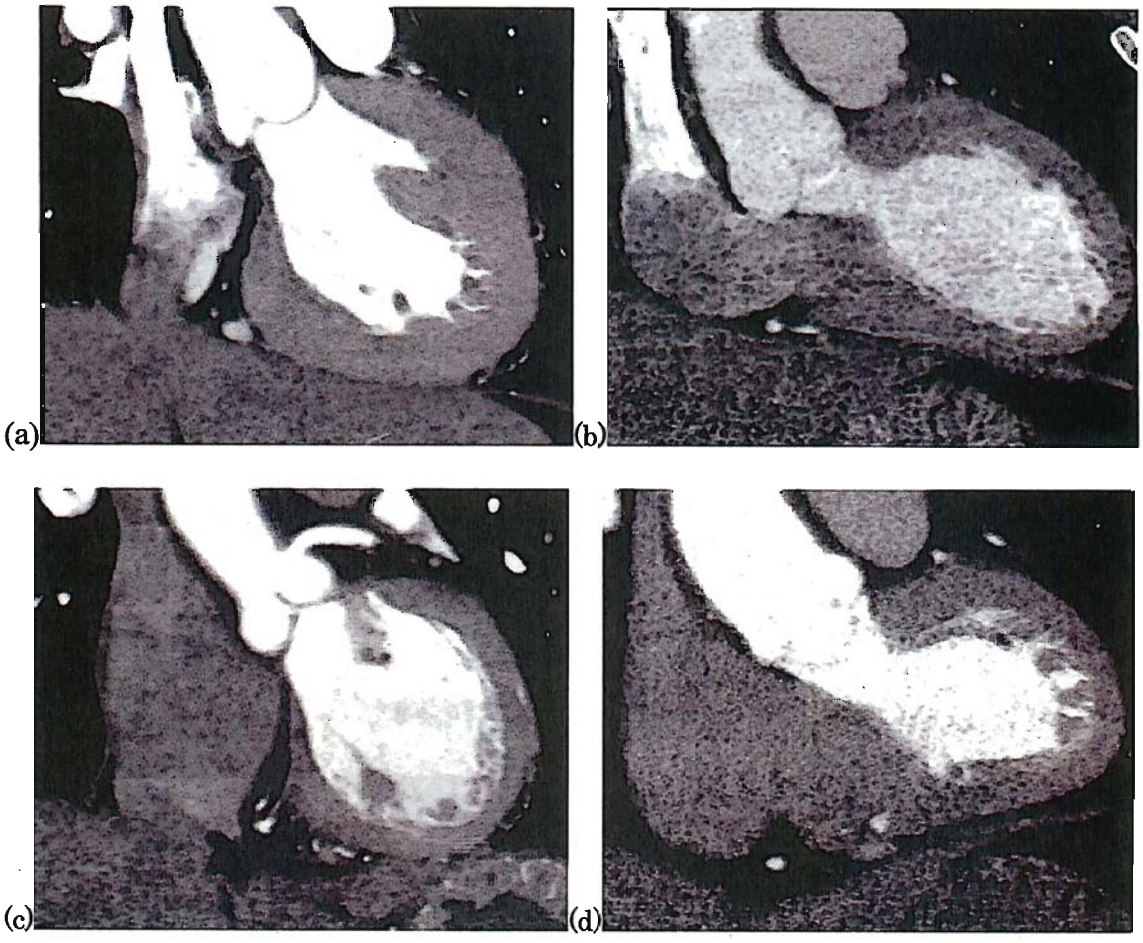

Figure 3. Multiplanar reformation of 64-detector CT images obtained with the 2 protocols in 4 representative cases illustrative of high- and low body weight patients.

(a) A 46-kg patient treated with protocol 1.

(b) An 80-kg patients treated with protocol 1.

(c) A 45-kg patient treated with protocol 2.

(d) A 78-kg patient treated with protocol 2.

There is almost no difference in the enhancement of the ascending aorta, irrespective of the protocol used.

Table 2 Success rate of adequate vessel enhancement

	Attenuation < 300HU	Attenuation >= 300HU
P1	5	25
P2	0	30

* Statistical significance of the successful rate of adequate vessel enhancement between the P1 and P2 ($p = .03$).

Table 3 Image Noise of each slice

Level	Protocol 1	Protocol 2	P value
Aorta (slice1)	32.0±8.0	25.8±6.0	< 0.01
Aorta (slice2)	30.8±8.2	26.2±6.7	0.02
interventricular septum (slice	27.0±8.0	22.6±7.4	0.03
interventricular septum (slice	23.5±9.5	24.6±10.5	0.68

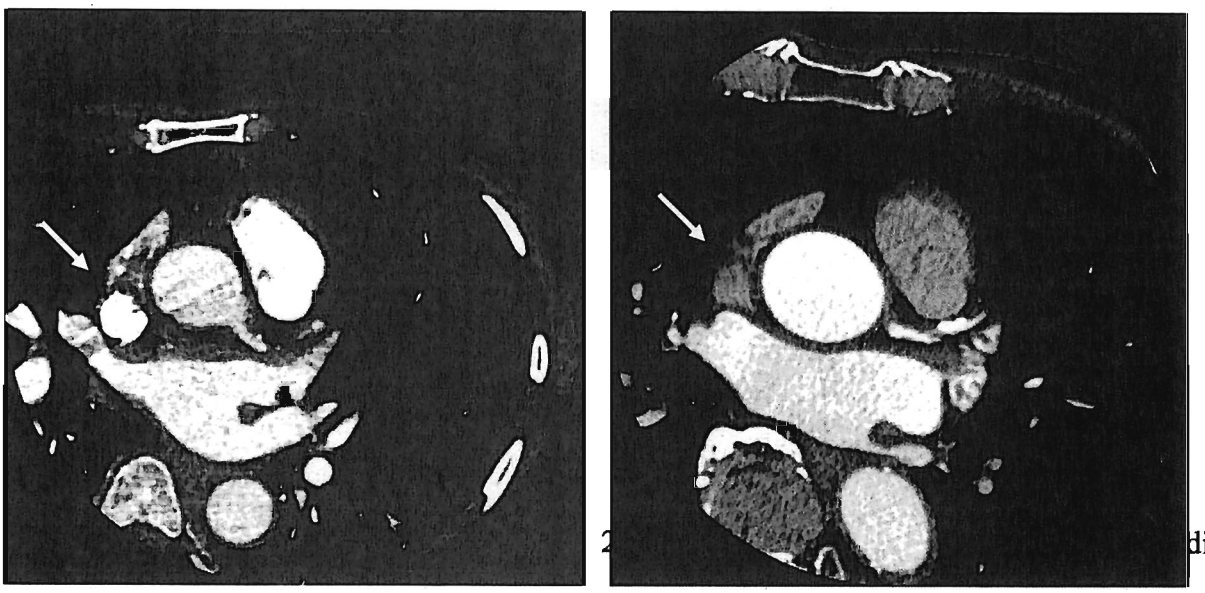

2 different injection protocols.

(a) A 60-kg patient treated with protocol 1. Note contrast "pooling" in the superior vena cava (arrow). Streak artifacts arising from the superior vena cava led to image-quality degradation.

(b) A 58-kg patient treated with protocol 2. Note contrast "wash-out" in the superior vena cava (arrow) and abatement of the image noise.

Figure Legends - Chapter III

Parameter	no-myocardial bridging (n= 56)	incomplete myocardial bridging (n=40)	complete myocardial bridging (n=34)	Total (n=130)	P Value
Age*	66.3±12.0	65.7±13.1	67.5±9.9	66.4±11.8	0.86
Sex (Male/Female)	33 /23	23 /17	28/6	84/46	0.02
Risk factors					
BMI*	23.2±3.4	23.5±2.8	23.4±3.0	23.4±3.1	0.44
Diabetes	27 (48.2%)	17 (42.5%)	16 (47.0%)	60 (46.2%)	0.69
Hypertension	34 (60.7%)	27 (67.5%)	20 (58.8%)	81 (62.3%)	0.44
Hyperlipidemia	22 (39.3%)	21 (52.5%)	11 (32.4%)	54 (41.5%)	0.08
Smoking	30 (53.6%)	15 (37.5%)	18 (52.9%)	63 (48.5%)	0.18

Table 1. Baseline Patient Characteristics

There were no significant differences in the baseline characteristics except for gender; of the 34 patients with complete myocardial bridging, 28 were males ($p<.05$).

Visual score	no-myocardial bridging (n= 56)	incomplete myocardial bridging (n=40)	complete myocardial bridging (n=34)
0	25 (44.6%)	13 (32.5%)	4 (11.8%)
1	10 (17.9%)	9 (22.5%)	8 (23.5%)
2	21 (37.5%)	18 (45.0%)	22 (64.7%)
mean ± SD	0.9±0.9	1.1±0.9	1.5±0.7

Table 2. Plaque Burden in the proximal segment of the LAD

The mean visual scores were 0.9 ± 0.9 for the no bridging group, 1.1 ± 0.9 for the incomplete-, and 1.5 ± 0.7 for the complete bridging group. The scores for plaque burden were significantly higher in the complete- than the no bridging group ($p<.05$). There was no statistically significant difference in the scores for the other pairs.

Visual score	no-myocardial bridging (n= 56)	incomplete myocardial bridging (n=40)	complete myocardial bridging (n=34)
0	36 (64.3%)	35 (87.5%)	30 (88.2%)
1	6 (10.7%)	4 (10%)	4 (11.8%)
2	14 (25%)	1 (2.5%)	0 (0%)
mean ± SD	0.6±0.9	0.2±0.4	0.1±0.3

Table 3. Plaque Burden in the middle segment of the LAD

The mean visual scores were 0.6 ± 0.9 for the no bridging group, 0.2 ± 0.4 for the incomplete- and 0.1 ± 0.3 for the complete bridging group. The scores assigned for plaque burden were significantly higher in the complete- and incomplete bridging group than in patients with no myocardial bridging ($p<.05$). There was no significant difference in the scores for the other pairs.

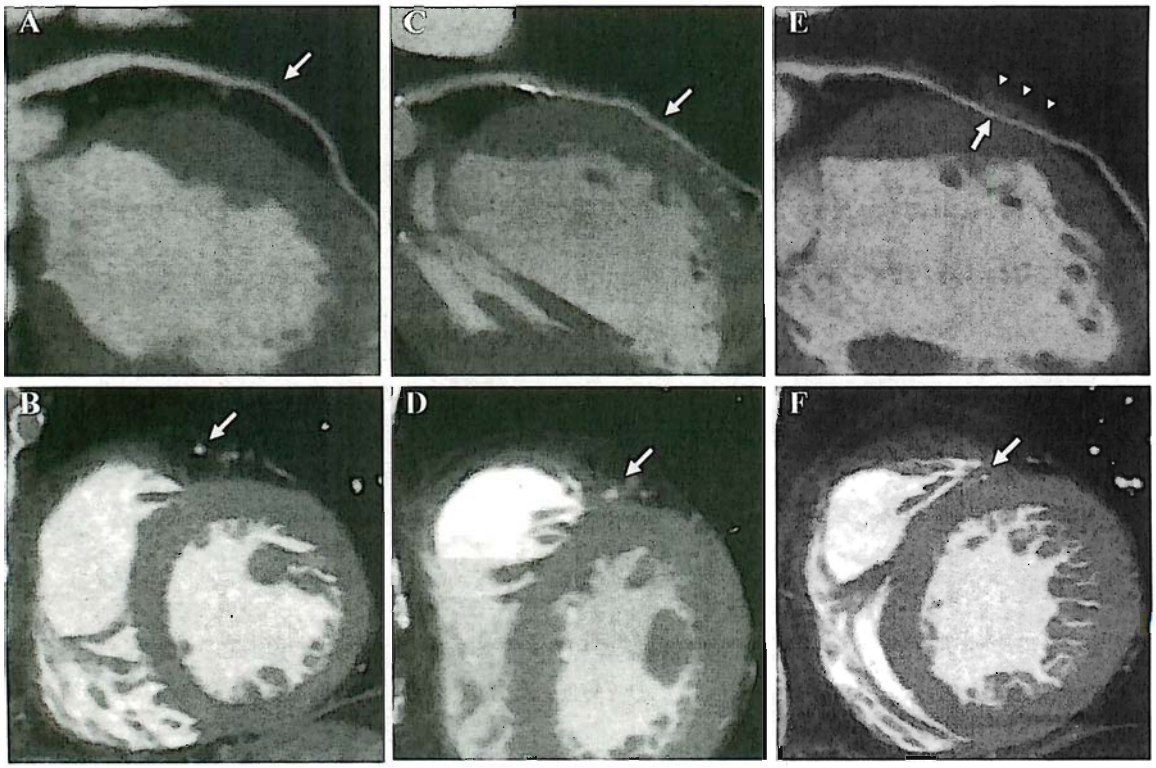

Figure 1. Examples of multiplanar reformation (MPR) and curved MPR (CPR) images of each group; no-bridging groups (A and B), incomplete bridging groups (C and D) and complete bridging groups (E and F).

Figure 1A and B. 62 year old Female with no-bridging. LAD is located on the epicardial surface of the heart, and surrounded by epicardial fat (arrows).

Figure 1C and D. 81 year old Female with incomplete bridging. A segment of LAD travels in the interventricular groove (arrows).

Figure 1E and F. 63 year old Male with complete bridging. A segment of LAD travels in the interventricular groove (arrows) and is covered by myocardium (arrow head).

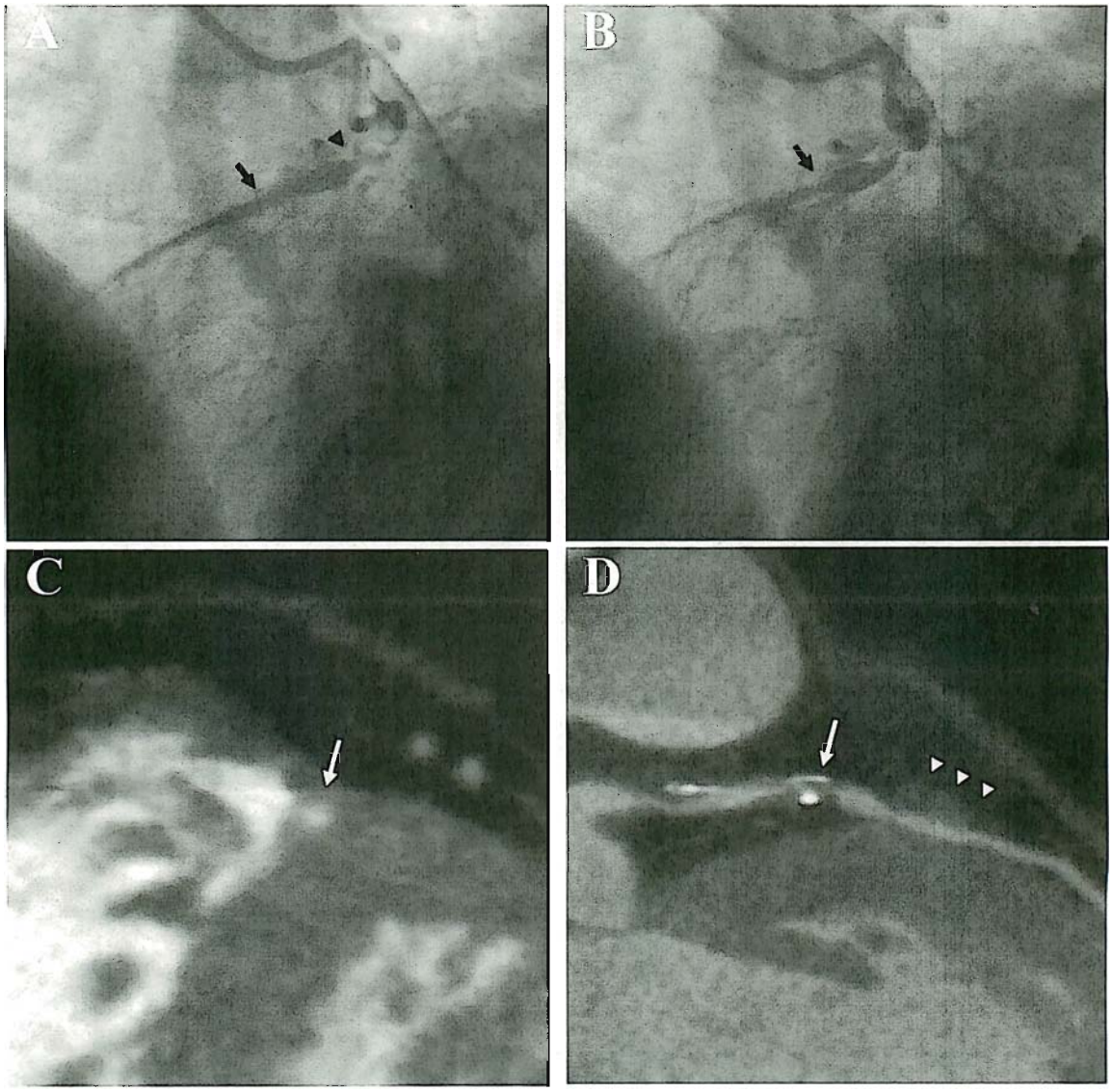

Figure 2. 51 year old Male with ischemic heart disease.

A and B. Conventional angiography in diastole (A) and systole (B) shows large thrombus in the proximal segment of LAD (arrow head) and 'milking effect' in the middle segment of LAD (arrow).

C and D. MDCT coronary angiography shows complete bridging (C, arrow), overlaying myocardium (arrow head) and large plaque (D, arrow) just proximal to the tunneled artery.